Published in final edited form as:
Biochemistry. 2013 April 23; 52(16): 2793–2809. doi:10.1021/bi3015983.

Effect of Calcium on the Oxidative Phosphorylation Cascade in Skeletal Muscle Mitochondria

Brian Glancy[1], **Wayne T Willis**[2], **David J Chess**[1], and **Robert S Balaban**[1]

[1]Laboratory of Cardiac Energetics, NHLBI, NIH, Bethesda, MD 20892

[2]School of Life Sciences, Arizona State University, Tempe, AZ 85287

Abstract

Calcium is believed to regulate mitochondrial oxidative phosphorylation, thereby contributing to the maintenance of cellular energy homeostasis. Skeletal muscle, with an energy conversion dynamic range of up to 100-fold, is an extreme case for evaluating the cellular balance of ATP production and consumption. This study examined the role of Ca^{2+} on the entire oxidative phosphorylation reaction network in isolated skeletal muscle mitochondria and attempted to extrapolate these results back to the muscle, *in vivo*. Kinetic analysis was conducted to evaluate the dose response effect of Ca^{2+} on the maximum velocity of oxidative phosphorylation (V_{maxO}) and the ADP affinity. Force-flow analysis evaluated the interplay between energetic driving forces and flux to determine the conductance, or effective activity, of individual steps within oxidative phosphorylation. Measured driving forces (extramitochondrial phosphorylation potential (ΔG_{ATP}), membrane potential, and redox states of NADH and cytochromes b_H, b_L, c_1, c, and a,a_3) were compared with flux (oxygen consumption) at 37°C. 840 nM Ca^{2+} generated a ~2 fold increase in V_{maxO} with no change in ADP affinity (~43 μM). Force-flow analysis revealed that Ca^{2+} activation of V_{maxO} was distributed throughout the oxidative phosphorylation reaction sequence. Specifically, Ca^{2+} increased the conductance of Complex IV (2.3-fold), Complexes I+III (2.2-fold), ATP production/transport (2.4-fold), and fuel transport/dehydrogenases (1.7-fold). These data support the notion that Ca^{2+} activates the entire muscle oxidative phosphorylation cascade, while extrapolation of these data to the exercising muscle predicts a significant role of Ca^{2+} in maintaining cellular energy homeostasis.

Keywords

metabolic homeostasis; bioenergetics; electron transport chain; cytochrome oxidase; thermodynamic stoichiometry

Exercise presents a severe challenge to energetic homeostasis in skeletal muscle as tissue-specific oxygen consumption rates can increase over 100-fold from rest to maximal aerobic exercise (1). Increases in skeletal muscle work rate are associated with modest decreases in the cytosolic ATP free energy (ΔG_{ATP}) primarily through increases in [ADP] and [Pi] (2-4).

Corresponding Author: Brian Glancy, NHLBI, NIH, 10 Center Dr Room B1D416, Bethesda, MD 20892, glancybp@nhlbi.nih.gov, Phone: 301-496-2679 Fax: 301-402-2389.

Supporting Information: Additional supplemental figures are available free of charge via the Internet at http://pubs.acs.org.

Since both muscle contraction and ion transport processes are dependent on ΔG_{ATP}, minimizing the reduction in ΔG_{ATP} during increases in energy demand is critical to the maintenance of normal cellular functions, such as ion gradients for signaling, as well as allowing peak muscle performance. Calcium (Ca^{2+}) release from the sarcoplasmic reticulum (SR) and subsequent binding to troponin C allows muscle contraction and the associated energy utilization to occur, while Ca^{2+} influx into mitochondria has been shown to result in increased energy conversion potential (5-9). This balanced activation of both energy conversion and utilization pathways has been proposed to play a key role in the maintenance of energetic homeostasis in contracting muscle (10-13).

Ca^{2+} has long been known to stimulate flux through the citric acid cycle by activation of pyruvate, isocitrate, and 2-oxoglutarate dehydrogenases (14). More recently, Ca^{2+} has also been shown to directly stimulate ATP production through activation of the F_1F_o-ATP synthase (9), and flux through Complex III of the electron transport chain (ETC) may also be stimulated by Ca^{2+} (15). Despite the importance of Ca^{2+} for both skeletal muscle contraction and activation of oxidative phosphorylation, few studies have examined the effects of Ca^{2+} on skeletal muscle mitochondrial energy conversion. Martin et al. (16) found that increasing Ca^{2+} lowered the respiratory control (RCR) and ADP/O ratios in isolated skeletal muscle mitochondria, though the free Ca^{2+} concentrations used in that study (0.4 – 19.1 μM) were tailored to answer questions about aging and apoptosis and not resting and exercising muscle (<0.05 – 1.5 μM) (17-19). Kavanagh et al. (6) reported that skeletal muscle mitochondria in the presence of Ca^{2+} have an increase in flux through the substrate oxidation pathway for NAD-linked fuels as well as the phosphorylation pathway regardless of fuel. However, the inhibitor titrations used by Kavanagh et al. (6) make it difficult to discern Ca^{2+} effects on the ETC from those on the substrate dehydrogenases and/or the ATP producing/transporting enzymes.

The purpose of this study was to determine the role of Ca^{2+} in modulating oxidative phosphorylation in isolated porcine skeletal muscle mitochondria. We hypothesized that Ca^{2+} would increase the maximum velocity of oxidative phosphorylation, as seen in other systems (8, 9, 15, 20), and that this effect would be the result of a distributed activation of reactions within the oxidative phosphorylation network. This was evaluated by establishing the dose response effect of Ca^{2+} on oxidative phosphorylation and performing force-flow analyses of the oxidative phosphorylation network using concurrent measures of the redox states of NADH and the cytochromes, the extramitochondrial free energy of ATP (ΔG_{ATP}), and mitochondrial membrane potential ($\Delta\Psi$) to estimate the effective conductance of several of the reaction steps of oxidative phosphorylation in the presence and absence of Ca^{2+}.

Experimental Procedures

Mitochondrial Isolation and Normalization

All procedures were approved by the National Heart, Lung, and Blood Institute Animal Care and Use Committee and performed in accordance with the guidelines described in the Animal Care and Welfare Act (7 USC 2142 § 13). Skeletal muscle mitochondria from the oxidative, porcine vastus intermedius were isolated using a Percoll gradient as described previously (21). Mitochondria were normalized to the optically-determined cytochrome a,a_3

(cyt a) content since this assay was very fast, did not require a standard curve, and provided the actual amount of mitochondrial oxidative phosphorylation complex in the sample independent of cytosolic contaminates. Cyt a content was measured as described previously (22), typically yielding a final mitochondrial suspension of 20 – 35 nmol cyt a/ml. Purified porcine skeletal muscle mitochondria contain ~1.0 nmol cyt a/mg protein (21).

Mitochondrial Respiration, NADH, and Membrane Potential

Mitochondrial oxygen consumption (J_o), NADH fluorescence, and membrane potential ($\Delta\Psi$) were measured simultaneously and continuously in a water-jacketed chamber maintained at 37°C as described previously (9, 23). Experiments were carried out with mitochondria (375 pmol cyt a) in a 1.5-ml final volume of respiration medium (RM) containing (in mM) 100 KCl, 50 MOPS, 20 glucose, 15 NaCl, 10 $MgCl_2$, 1 EGTA, and 0.2% w/v BSA, pH 7.0. J_o was measured using a Clark electrode and an oxygen solubility of 199 nmol/ml at 37°C (24).

NADH reduction level was calculated relative to the fully oxidized (Ca^{2+}-depleted mitochondria, no added substrates, with ADP and Pi) and fully reduced (mitochondria with added substrates and Ca^{2+} at anoxia) states. $\Delta\Psi$ was determined based on the distribution of the lipophillic cation TPP^+ across the inner mitochondrial membrane using a TPP^+ sensitive microelectrode (KWIKTPP, World Precision Instruments). TPP^+ binding to mitochondria was accounted for as described previously (9). With 10 mM Pi in the RM for all experiments along with sodium in the medium, the contribution of the pH gradient (ΔpH) to the protonmotive force (ΔpH + $\Delta\Psi$) was assumed to be insignificant (25).

Experimental Conditions

For all respiration experiments, mitochondria were incubated in RM at 37°C in the presence of sodium and in the absence of exogenous substrates or energy phosphates in order to deplete endogenous Ca^{2+} from the mitochondrial matrix (5, 6, 9). After the depletion step, 10 mM Pi and 0.13 mM ADP were added, followed by glutamate (G, 10 mM) and malate (M, 1 mM) ± Ca^{2+}. Addition of fuel (G+M) initiated a submaximal increase in J_o followed by a subsequent transition to State 4 J_o. For experiments designed to measure maximal J_o, State 3 was then elicited with a bolus of 1.3 mM ADP which resulted in consumption of all the oxygen in the chamber providing the fully reduced state (anoxia). Free Ca^{2+} concentrations were made using the calculator programs of Fabiato and Fabiato (26) translated to Labview VIs (National Instruments Corp, Austin, TX) by Reitz and Pollack (27).

Steady-state, intermediate J_o was attained using a progressive creatine kinase (CK) energetic clamp (28), we have recently modified (29). Briefly, by utilizing a large total creatine pool, excess CK, a known [ATP], and the CK equilibrium constant (K_{CK}, 150 (30)), the extramitochondrial ATP/ADP ratio, and thus, free energy of ATP hydrolysis (ΔG_{ATPe}) can be calculated from the added phosphocreatine (PCr)/creatine (Cr) ratio:

$$\Delta G_{ATPe} = \Delta G_{ATP} \circ -2.3 * RT * \log([PCr] * K_{CK} / ([Cr] * [Pi])) \quad (1)$$

where $\Delta G_{ATP}°$ is the standard ΔG_{ATP} (-7.592 kcal/mol), R is the gas constant (1.987 $cal \cdot K^{-1} \cdot mol^{-1}$), and T is temperature (310°K). Mitochondria oxidizing G+M at State 4 were given 2.5 mM PCr, 5 mM Cr, 5 mM ATP, and 75 U/ml CK, resulting in a J_o of ∼2/3 of State 3. Subsequent additions of PCr (to 3.75, 5, 7.5, and 10 mM) were made to slow J_o to ∼1/3 of State 3.

Additional experiments with pyruvate were conducted similar to those from Messer et al. (28). Briefly, mitochondria in the presence of saturating M were exposed to the CK clamp as described above with a PCr/Cr ratio of 0.25. Pyruvate was then titrated in stepwise at 10, 25, 50, 100, and 500 μM to increase respiration. The novel aspect of this experiment was that upon reaching a steady state with 500 μM pyruvate, stepwise additions of PCr were then made to slow J_o. Thus, in a single experiment, J_o was changed by both “Push” (pyruvate titration) and “Pull” (CK clamp) mechanisms.

Mitochondrial Optical Absorption

A system was developed from our earlier work with an integrating sphere to minimize the effects of light scattering on the visible spectrum of mitochondrial suspensions (23). Our current implementation permits studies on well-mixed samples at physiological temperatures with a complete linear regression analysis of the chromophores of oxidative phosphorylation (31). Briefly, a 6-inch integrating sphere (model RTC-060-SF, LabSphere, Inc., North Sutton, NH, USA) was used with a custom-designed, 1.2-cm diameter, cylindrical, water-jacketed, center-mounted chamber to hold the mitochondrial suspension. The volume used in this chamber was 2 ml. The sample was uncapped and oxygen consumption measurements in the chamber were not attempted due to the optical interference of electrodes. All oxygen consumption data was collected in parallel in a dedicated polarography chamber at the same temperature. All experiments were conducted at 37°C. White light (model CS-16-500, Jobin-Yvon, Inc., Spex® Forensics Division, Edison, NJ, USA) was impinged on the sample and the absorbed light was collected via a fiber optic using the sampling port on the sphere. Rapid-scanning optical spectra (1 spectrum/100 msec) were collected using a photodiode array (model QE-65000, Ocean Optics, Inc.) from ∼300 to 800nm. Analysis was conducted on the β and α bands of the cytochromes from the 466 to 630nm region since this provided the best discrimination of the absorbance bands (31).

Data analysis was performed by completely fitting the absorbance difference spectra to 7 reference difference spectra for FAD, cytochrome b_H, cytochrome b_L, cytochrome c_1, cytochrome c, cytochrome a_3 peroxy form (a_{607}), cytochrome a_3 ferryl form (a_{580}), and a simple linear term for baseline corrections as previously described using linear regression fitting (31). The fully oxidized state was taken as mitochondria in the absence of carbon substrates and the addition of ADP and Pi. The fully reduced state for FAD and cytochromes b_H, c_1, c, and a_{607} was obtained by adding a small amount of sodium hydrosulfite at the end of the experiment. Cytochromes b_L and a_{580} were most reduced under State 4 conditions, thus, State 4 was considered as full reduction for these two species. Cytochrome a_{580} reduction level was then normalized to total cyt a content assuming a 1:2 extinction coefficient ratio for a_{580} and a_{607}, respectively (32, 33).

Driving Forces and Pathway Conductances

In this study, the force-flow behavior for different regions of the oxidative phosphorylation network was used to estimate the effective conductance (or resistance) of each region during active oxidative phosphorylation. This is in contrast to studies on isolated protein complexes in native gels or which alter the pathway using inhibitor titrations where oxidative phosphorylation is not proceeding under normal conditions. To accomplish this task, the oxidation/reduction (redox) potentials (E_h) of the products and reactants of a reaction segment, as well as $\Delta\Psi$ when appropriate, must be determined for the driving force, while J_o provides the flux for all of the elements. Mitochondrial Complex E_h for redox pairs was calculated as:

$$E_h = E_m + 2.3*(RT/nF)*\log([\text{oxidized}]/[\text{reduced}]) \quad (2)$$

where E_m is the midpoint potential (-320 mV for NAD/NADH, +230 for cyt c_1, +270 mV for cyt c, +280 mV for cyt a_{607}, and +820 mV for O_2/H_2O (34-37)), n is the number of electrons to be transferred, and F is the Faraday constant (23.062 cal·mV^{-1}·mol^{-1}). Free energies (ΔG) were calculated assuming that a single NADH donates 2 electrons (n) to the ETC resulting in 10 protons pumped (m) which, in turn, yields 2.7 ATP (p):

$$\Delta G_{redox} = -nF(\Delta E_h + z\Delta\Psi) \quad (3)$$

$$\Delta G_{\Delta\Psi} = -mF\Delta\Psi \quad (4)$$

$$\Delta G_{ATP} = p\Delta G_{ATPe} \quad (5)$$

where Eq. 3 is used for the free energy driving electron transfer with ΔE_h as the redox potential difference and z as the relative distance across the mitochondrial inner membrane relative to the matrix side between two redox pairs, Eq. 4 is used for the free energy associated with pumping protons across the mitochondrial inner membrane, and Eq. 5 is used for the stoichiometric free energy of ATP hydrolysis. For electron transfer steps within the ETC, m was varied according to the number of protons moved across the mitochondrial inner membrane between the respective electron donors and acceptors, and z was assumed to be 1, 0, 0, and -1 for electron transfer between NADH and cyt c_1, cyt c_1 and cyt c, cyt c and cyt a_{607}, and cyt a_{607} and O_2, respectively, yielding a value of 0 for electron flow down the entire ETC.

Flux down an oxidative phosphorylation pathway was assumed to vary according to the thermodynamic driving forces acting on it using classical irreversible thermodynamic approaches (38, 39):

$$J = L(\Delta G_1 - \Delta G_2) \quad (6)$$

where J is the flux down the pathway, L is the phenomenological transport coefficient of the reaction, and ΔG_1 and ΔG_2 are the driving forces acting on the front and back ends of the pathway, respectively. For the purposes of this discussion we will refer to the transport coefficient, L, as a "conductance" since many of the reactions we are evaluating involve the displacement of charged species. Simultaneous measurement of oxygen flux (J_o) and the thermodynamic driving forces for oxidative phosphorylation (ΔG_{redox}, $\Delta G_{\Delta\Psi}$, and ΔG_{ATP}) thus allows for the calculation of the conductances of the ETC (ΔG_{redox} - $\Delta G_{\Delta\Psi}$), ATP synthesis/transport ($\Delta G_{\Delta\Psi}$ - ΔG_{ATP}), and complete oxidative phosphorylation pathways (ΔG_{redox} - ΔG_{ATP}). Under conditions of saturating oxidative substrates, we considered the free energy associated with the added fuel to be constant. As such, we were also able to calculate the conductance of the fuel transport/dehydrogenase pathway ($\Delta G_{Fuel} - \Delta G_{NADH}$) and of the complete mitochondrial energy conversion process ($\Delta G_{Fuel} - \Delta G_{ATP}$) using the ΔG_{NADH} and ΔG_{ATP} relationships with J_o, respectively.

Stoichiometries

The ratios of protons pumped across the inner membrane per electron passed (H^+/e^-) were measured using the force ratio (40-42). Briefly, the ratio of the respective thermodynamic forces was plotted against J_o, and from the resultant linear relationship, the force ratio at zero flux (x-intercept) could be extrapolated. Under equilibrium conditions, plugging Equations 3 and 4 into Equation 5 and rearranging arrives at the following:

$$m/n = \Delta E_h/\Delta\Psi + z \quad (7)$$

where m/n is the H^+/e^- ratio. The experimentally-determined stoichiometries were then compared to those used in the ΔG calculations to provide a measure of validity.

Statistical Analysis

For the Ca^{2+} titration experiments, significant differences were assessed using a repeated measures ANOVA with a Tukey-Kramer multiple comparisons post-hoc test. Differences in slopes between Ca^{2+} and no Ca^{2+} conditions were assessed using a two-tailed, paired Student's t-test. A P-value of 0.05 was used to determine statistical significance.

Results

Maximal Respiration

State 3 J_o as well as State 3 and 4 NADH levels rose with increasing [Ca^{2+}] up to 840 nM, beyond which a plateau occurred (Figure 1). The initial increase in State 3 with Ca^{2+} was linear with a slope of 0.33 nmol O_2/min/nmol cyt a/nM Ca^{2+}. The optimal Ca^{2+} dose (840 nM) for respiration resulted in a 1.8-fold increase in State 3 J_o (405.9 ± 12.6 nmol O_2/min/nmol cyt a) compared to that with no Ca^{2+} (226.8 ± 17.5 nmol O_2/min/nmol cyt a). Surprisingly, the optimal Ca^{2+} dose had no effect on ΔΨ at State 3 and State 4 despite the large increase in NADH and J_o. This result implies that the effects of Ca^{2+} cannot be through alterations in ΔΨ alone as other processes must be affected.

The mitochondrial isolation process typically results in mitochondria with high endogenous levels of Ca^{2+} (43, 44). Depletion of endogenous calcium for these experiments was achieved through a 6 minute mitochondrial incubation period at 37°C without added substrates and in the presence of 15 mM sodium (to stimulate Na^{+}/Ca^{2+} exchange) which we have previously shown to remove nearly all Ca^{2+} from the mitochondrial matrix (45). This incubation step resulted in a State 3 J_o that was 49% of the rate without incubation or NaCl (Table 1). Addition of Ca^{2+} after the incubation period resulted in a State 3 J_o that was 88% of the rate without incubation which is consistent with the notion that the effects of the incubation period are primarily due to a depletion of Ca^{2+}.

Steady-State, Intermediate Respiration

A representative trace of a CK clamp experiment is shown in Figure 2, and the resultant linear relationship between ΔG_{ATPe} and J_o is presented in Figure 3A (3, 46, 47). A roughly two-fold increase in respiration was observed with calcium at each clamped ΔG_{ATPe} value (Figure 3 A). Therefore, the ability to produce ATP with fixed substrate and product concentrations was increased by Ca^{2+}. This result implied that the V_{max} of the mitochondria for producing ATP was increased by Ca^{2+}. To confirm this notion, these data were reformulated to extract the affinity of oxidative phosphorylation for ADP. In Figure 3B, the dose response curve of [ADP] versus J_o reveals typical saturating kinetics. The Eadie-Hofstee plot in Figure 3C demonstrates that the increase in J_o with Ca^{2+} was not due to a change in ADP affinity, ∼43 μM, but rather, due to a doubling of the V_{max} from ∼200 to ∼425 nmol/min/nmol cyt a, consistent with the data presented in Figure 1. It is important to note that combining the increase in V_{max} due to Ca^{2+} with the change in ADP from resting muscle (∼5 μM) to that during modest concentric exercise (∼25 μM) in humans (48) can explain an ∼7-fold increase in respiration rate. These physiological points are highlighted in Figure 3B and the combined effects of Ca^{2+} and ADP are further developed in the Discussion.

The remaining studies focused on isolating the elements within oxidative phosphorylation responsible for the increase in V_{max} by Ca^{2+}. To evaluate the contribution of different steps in the oxidative phosphorylation network, the phenomenological conductance was determined for each step where the net driving forces could be measured. The primary potential energy for oxidative phosphorylation, especially with the substrates we utilized, is the free energy in NADH which is then converted into $\Delta\Psi$. The force:flow relationships for these parameters are presented in Figure 4 where the convention of the force, net NADH or $\Delta\Psi$, is plotted on the X-axis, and flow, J_o, is plotted on the Y-axis. The force:flow relationships for NADH and $\Delta\Psi$ were linear for both the control and Ca^{2+} conditions. Ca^{2+} increased the force:flow slopes by ∼0.7- and 2.1-fold for NADH and $\Delta\Psi$, respectively (Table 2). These data are consistent with previous observations in porcine heart mitochondria (9). The relationships in Figure 4 provide only a measure of the balance between production and utilization of the respective free energies, NADH or the resulting $\Delta\Psi$, thus, many different parameters could contribute to the Ca^{2+}-induced changes in total velocity and slope, including dehydrogenase activity, ADP kinetics on F_1F_oATPase velocity, or any alterations within the ETC. Thus, to determine the specific locations of Ca^{2+} sensitivity, we used the free energy differences measured across various spans of the

mitochondrial energy conversion pathway along with J_o to determine the conductance, or reciprocally, the resistance to energy flow of each span. Figure 5 depicts the thermodynamic driving forces measured and the energy conversion steps for which conductances were calculated.

The conductance of the entire oxidative phosphorylation cascade, L_{Oxphos}, was determined by plotting J_o versus $((\Delta G_{NADH} - \Delta G_{O2}) - \Delta G_{ATP})$, the potential energy across the oxidative phosphorylation process. It is important to note that since the ΔG_{NADH} is included in this calculation, the effects of dehydrogenase activation are eliminated from this force:flow relationship which is presented in Figure 6A. The overall L_{Oxphos} increased 2.0-fold in the presence of Ca^{2+}. These data are consistent with the notion that the ability of oxidative phosphorylation to generate ATP at a given free energy is improved in the presence of Ca^{2+}.

It has been previously established that Complex V maximal activity is increased by Ca^{2+} (9). We confirmed that the ATP synthesis mechanism, L_{ATPase}, which includes both Complex V and the adenylate nucleotide translocase (ANT), was activated by Ca^{2+} by plotting J_o versus $\Delta\Psi$-ΔG_{ATP} in Figure 6B. The calculated L_{ATPase} increased by a factor of 2.4 in the presence of Ca^{2+} (Table 2) consistent with previous results in the porcine heart (9) and recent biochemical analysis (49).

To eliminate L_{ATPase} from the conductance calculation, we determined the conductance of the electron transport chain, L_{ETC}, using $((\Delta G_{NADH} - \Delta G_{O2}) - \Delta G_{\Delta\Psi})$ to take into account only the free energy driving the ejection of charge and not ATP synthesis. As seen in Figure 6C, L_{ETC} was increased 2.4-fold in the presence of Ca^{2+}. These data suggest that Ca^{2+} is activating the ETC independent of effects on Complex V or dehydrogenases.

Using the cytochrome spectra as shown in Figure 7, we could isolate different regions of the ETC to examine whether Ca^{2+} was altering the reaction kinetics. Force:flow relationships for cytochromes b_H, b_L, c_1, c, and a peroxy (a_{607}) and ferryl (a_{580}) with and without Ca^{2+} are shown in Figure 8A-F. Ca^{2+} caused a greater reduction of all cytochromes with the exception of b_L. However, the slope of the relationship between b_L and J_o was increased 2.7-fold by Ca^{2+}. The thermodynamic relationships and the chromophores detected provided the differential driving forces for the flux between NADH and cyt c_1 (for calculating L_{CI+III}), cyt c1 to cyt c (for calculating L_{c1c}), cyt c and cyt a_{607} (for calculating L_{CIVa}) as well as cyt a_{607} with oxygen (for calculating L_{CIVb}). The use of cyt b redox forms for calculating a driving force was complicated by the Q cycle, thus, Complex III was lumped with Complex I in L_{CI+III}.

The calculations of the conductance of the different portions of the ETC are presented in Figure 9A-D. All of the Complexes of the ETC were activated by Ca^{2+} with L_{CI+III} increasing 2.2-fold (Figure 9A), L_{CIVa} increasing 2.4-fold (Figure 9C) and the terminal reaction with oxygen, L_{CIVb}, increasing 2.2-fold (Figure 9D). These calculations suggest that Ca^{2+} had a ubiquitous effect on the activity of the electron transport system consistent with activation within Complex I/Complex III and the interactions within Complex IV.

Resistance to Mitochondrial Energy Conversion

By considering mitochondrial energy conversion as flux across a series of resistors (see Figure 5), we were able to calculate the contribution of each span of the energy conversion process to the total resistance to energetic flux. These results are shown in Table 3 where, in the absence of Ca^{2+}, Complex IV was determined to provide the most resistance to flux followed by Complex I+III, ATP production/transport, and fuel transport/dehydrogenases. Note that the resistance from cyt c to cyt a_{607} was considered negligible as $\Delta G_{cyt\ c\ -\ cyt\ a607}$ became more positive as J_o increased (Figure 9C) suggesting this reaction provides no flux control. Resistance between cyt c_1 and cyt c was also omitted from this analysis as there was little change in this free energy difference with neither a positive or negative relationship to flux (Table 2). Despite increasing conductances throughout the entire mitochondrial energy conversion pathway, Ca^{2+} addition caused a shift in the relative contribution to resistance away from the ETC (both Complex I+III and Complex IV).

Stoichiometries

Measuring the force ratios for the spans of the ETC provided validation for the stoichiometries chosen for making the free energy, and thus, conductance calculations described above. The ∼10% difference between measured and used values in Table 4 suggest that the numbers of electrons (n) and protons (m) were correctly assigned when using Equations 3 and 4 for the relationships depicted in Figures 6 and 9 and Tables 2 and 3.

Discussion

Steady-state Kinetic Analysis

Skeletal muscle free Ca^{2+} levels are typically less than 50 nM at rest and, at the onset of exercise, can transiently rise to 0.5 – 1.5 μM, depending on both intensity and modality (17, 18, 50). Using the reported skeletal muscle values as a guide, Ca^{2+}- depleted skeletal muscle mitochondria were incubated with concentrations up to 1.5 μM to determine the steady-state kinetic relationship between Ca^{2+} and State 3 and State 4 J_o, NADH, and $\Delta\Psi$, as well as the optimal Ca^{2+} dose to stimulate oxidative phosphorylation (Figure 1). The kinetic relationship to Ca^{2+} was similar between J_o and NADH, with both being maximally stimulated at 840 nM Ca^{2+}. Thus, the optimal Ca^{2+} dose for oxidative phosphorylation in isolated mitochondria is similar to that in exercising muscle, and, as a result, the Ca^{2+} levels used in this study may offer some insight into the Ca^{2+} activation of mitochondria in the transition from rest to exercise. It should be noted that temporal kinetics of Ca^{2+} exposure to the mitochondria in these studies with constant step changes is much different than the transient nature of cytosolic Ca^{2+}, *in vivo*. Thus, these steady state, *in vitro* kinetics can only be estimates of the *in vivo* conditions. Further kinetic analysis revealed that the increase in State 3 J_o with Ca^{2+} was the result of an increase in the apparent V_{max} of oxidative phosphorylation and not due to changes in ADP affinity (Figure 3C) as previously shown by Scaduto's group in heart mitochondria (8). However, since we used saturating concentrations of carbon substrates and a limited number of substrates, we cannot reach conclusions regarding carbon substrate affinity changes to Ca^{2+}. The remainder of the study focused on unraveling the mechanism of the Ca^{2+}-induced V_{max} increase in skeletal muscle mitochondria under these conditions.

Force:Flow Analysis

Simultaneous measurement of J_o, $\Delta\Psi$, and the NADH and cytochrome redox states at several different respiration rates allows for a novel evaluation of the impact of Ca^{2+} on metabolic flux and thermodynamic driving forces. The CK clamp provides mitochondria with extramitochondrial ΔG_{ATP} and $[ADP_f]$ values similar to those observed in human skeletal muscle *in vivo* (48, 51, 52). Thus, we were able to examine the effects of Ca^{2+} in an environment which may more closely approximate *in vivo* conditions compared to experiments using inhibitors and/or excess ADP.

Initial force:flow analyses examined the effect of Ca^{2+} on the conductance of the overall mitochondrial energy conversion cascade (L_{Mito}) by measuring the slope of the relationship between flux (J_o) and the difference between the forward (ΔG_{Fuel}) and reverse (ΔG_{ATP}) driving forces (Eq. 6 and Figure 5). Since ΔG_{Fuel} is assumed to be constant at the high substrate concentrations used, (ΔG_{Fuel} - ΔG_{ATP}) reduces to ΔG_{ATP} for this analysis. Using this simplification, the 2.0-fold increase in the $J_o/\Delta G_{ATP}$ slope shown in Figure 3A represents a 2.0-fold increase in L_{Mito}, nearly identical to the Ca^{2+}-induced increase in State 3 J_o discussed above. However, L_{Mito}, much like State 3 J_o, gives only a global view of the effect of Ca^{2+} on oxidative phosphorylation with no information on the specific sites that are affected. To remove the influence of fuel transportation and substrate dehydrogenases on L_{Mito}, we used the NADH redox status along with ΔG_{ATP} to calculate L_{Oxphos}, or the conductance of the oxidative phosphorylation reactions. Just as with L_{Mito}, Ca^{2+} caused a 2.0-fold increase in L_{Oxphos} (Figure 6A). Thus, oxidative phosphorylation was activated by Ca^{2+} independent of the well known effects of Ca^{2+} on dehydrogenases and substrate transport (53). We then split L_{Oxphos} into two separate elements, the combination of Complex V and ANT (ATP production/transport, L_{ATPase}) and the ETC (L_{ETC}), by using the measured intermediate, $\Delta\Psi$. L_{ATPase} was increased 2.4-fold by Ca^{2+} (Figure 6B) similar to previous reports demonstrating that Ca^{2+} activates cardiac Complex V (9, 49) and in skeletal muscle where Ca^{2+} activated the phosphorylation subsystem (6).

The conductance of the ETC, L_{ETC}, was also increased 2.4-fold by Ca^{2+} (Figure 6C). Since a pathway with greater conductance necessitates lower driving forces to achieve a given flux, and reactive oxygen species (ROS) production has been correlated with ETC driving forces (54), the increased conductance of the ETC with Ca^{2+} levels typical of exercising muscle may suggest a role for Ca^{2+} in minimizing ROS production upon the onset of exercise. Indeed, though Ca^{2+} given to inhibited mitochondria or in supraphysiologic doses causes an increase in ROS production (55), control mitochondria produce less ROS from Complexes I and III when given physiological levels of Ca^{2+} (56, 57).

Recent advancements in optical absorbance spectroscopy (31) have allowed for measurement of the status of individual complexes of the ETC without the use of artificial electron donors/acceptors or inhibitors and under conditions similar to those typically used in mitochondrial respiration studies. We employed these methods together with the force:flow analyses described above to determine the conductances of individual elements within the ETC. Surprisingly, we found that Ca^{2+} activated nearly every step within the ETC (Figure 9) with a 2.2-fold effect on L_{CI+III}, a 2.4-fold effect on L_{CIVa}, and a 2.2-fold effect

on L_{CIVb}. Unfortunately, we were unable to measure the redox status of ubiquinone which precluded the separation of Complexes I and III. However, based on our measurements of the redox status of cytochrome b_H and the proposed equilibrium between b_H and ubiquinone (58-60), we can predict that the Ca^{2+} effect on L_{CI+III} would be shared by both Complex I and Complex III. There have been few other reports on a Ca^{2+} stimulation of the ETC. Bender and Kadenbach (61) showed that Ca^{2+} recovered the inhibition of Complex IV activity by cAMP in bovine liver mitochondria, however, Ca^{2+} had no effect when cAMP was not present nor did it directly activate the isolated enzyme. Murphy et al. (15) suggested that the Ca^{2+} sensitivity of rat liver mitochondria was largely due to activation of flow through Complex III, but not Complex IV. However, Murphy et al. (15) reported a Ca^{2+}-stimulated maximal flux through Complexes III and IV (from ubiquinone to O_2) that was more than twice as high as the flux through Complex IV alone (from TMPD + ascorbate to O_2), suggesting that maximal Complex IV flux was not attained with TMPD + ascorbate as substrate in that study.

To our knowledge, the current broadband, spectroscopic approach is the first report of Ca^{2+} activation of multiple steps within the ETC. This activation of the ETC by Ca^{2+} may significantly contribute to the Ca^{2+} stimulation of ATP production during exercise. Hogan's lab recently found that a ‘priming’ bout of contractions removed an apparent limitation to flux caused by the ETC at the onset of contractions in an isolated single muscle fiber (62). These authors speculated that an increase in mitochondrial Ca^{2+} may have been responsible, at least in part, for the removal of the limitation to flux by the ETC, though Ca^{2+} levels were not specifically measured (62).

Network Thermodynamic Analysis

By calculating the conductances for sequential steps within the mitochondrial energy conversion cascade, we are also able to treat the system as a series of resistors where the resistance of each part is the reciprocal of its conductance. The total resistance of the series of reactions is then equal to the sum of the individual resistances within the system. This approach is similar to network thermodynamic approaches used for modeling multiple reaction steps in a metabolic cascade (63, 64). Further, we can calculate the resistance of each individual element as a percentage of the total resistance and examine whether Ca^{2+} alters the distribution of resistances within the energy conversion elements. Ca^{2+} addition resulted in a 1.9-fold decrease in the total resistance to mitochondrial energy conversion as well as a decrease in the resistance of each element (Table 3). However, the distribution of the resistances within the reaction series was altered by Ca^{2+}. The ETC contributed 64.8% of the total resistance to flux in the absence of Ca^{2+}, while the presence of Ca^{2+} reduced the contribution of the ETC to 51.7% of the total resistance to energy conversion. Despite the well-known effects of Ca^{2+} on increasing the activity of substrate dehydrogenases (7, 65), Ca^{2+} trended towards an increase ($p=0.09$), not decrease, in resistance of the fuel transport/substrate dehydrogenase pathway relative to the other components of mitochondrial energy transfer (Table 3). Thus, while Ca^{2+} did activate fuel transport/substrate dehydrogenases ($L_{Fuel/DH}$, Table 2), the effects were relatively greater on downstream pathways. This was not surprising, however, as it was recently pointed out that Ca^{2+} stimulation of respiration cannot be explained by activation of dehydrogenases alone (53).

The data in Table 3 also suggest that Complex IV and Complex V and/or ANT are critical sites of flux control within mitochondria respiring at intermediate rates, as these sites make the greatest contribution to the total mitochondrial resistance to energy conversion. Complex IV, Complex V, and ANT have each previously been reported as important loci of flux control in heart mitochondria (66-68), though the simulations of Korzeniewski and Mazat (69) suggested that, in skeletal muscle mitochondria, these three sites have little or no flux control during intermediate respiration. However, the hexokinase-ATPase system utilized by Korzeniewski and Mazat assumed 85% of the flux control during intermediate respiration with an additional 8% coming from the proton leak, leaving little room for flux control by any mitochondrial enzyme. The CK energy clamp system used here exerts no flux control itself (68), thus allowing for greater sensitivity in detecting the relative control of mitochondrial sites over energy conversion (70).

The observation that multiple steps of oxidative phosphorylation are regulated by Ca^{2+} is consistent with previous control strength analyses, using the approach of Kascer and Burns (71), finding that the control of oxidative phosphorylation is highly distributed under phosphorylating conditions (72-74). These studies used inhibitor titrations of different steps in the reaction series to establish if “excessive” activity was present and estimate the control strength of a given step based on the overall flux sensitivity to inhibitor action. These titrations, which did not compensate for changes in reaction driving forces as done here and which relied on the specificity of complex inhibitors, also revealed that Complex IV, ANT, and other steps within the ETC all contribute to the overall rate limitation of State 3 oxidative phosphorylation. In the absence of large changes in metabolite or intermediate concentrations, shared flux control among many sites within the energy conversion process necessitates a coordinated modulation of each site in order to achieve the large increases in flux observed *in vivo* (75). This theoretical prediction was bolstered by the *in silico* results of Korzeniewski (11, 76, 77) which, using a simplified model of oxidative phosphorylation, suggested that the V_{max}'s of the entire mitochondrial energy conversion process should be modulated by an external signal consistent with notions previously presented by Balaban (10) and Hochachka and Matheson (78) based on experimental data. Although previous cellular and whole tissue studies have found both pyruvate dehydrogenase (PDH) and Complex V to be activated by the onset of contractile work (49, 66, 79), experimental evidence for simultaneous, multi-site modulation by an external effector has been limited (6, 9, 80). The near ubiquitous activation across the mitochondrial energy conversion cascade observed here suggests that Ca^{2+} may play a role in the stimulation of oxidative phosphorylation *in vivo* contributing to the near metabolic homeostasis observed. However, the molecular mechanism for this effect is yet to be fully elucidated with the exception of a few dehydrogenases.

Contribution of Conductance and Driving Force to Flux

The force:flow and network thermodynamic analyses discussed above were done under the assumption that energetic flux can be explained by Ohm's Law. In other words, the current (J_o) must be equal to the voltage (ΔG) multiplied by the conductance (L) (Eq. 6). The linearity displayed in Figures 3, 4, 6, and 9 suggests that this was a valid assumption for nearly all steps within the oxidative phosphorylation cascade. With the establishment of flux

as the product of driving force and conductance, we can then determine how much of the increase in flux due to Ca^{2+} can be attributed to a change in driving force versus a change in conductance. Ca^{2+} caused an average 2.01-fold increase in J_o (Figure 3A) when comparing mitochondria provided the same extramitochondrial conditions (fuel and ΔG_{ATP}). The driving force for oxidative phosphorylation ($\Delta G_{NADH} - \Delta G_{ATP}$) increased on average by only 1.03-fold with Ca^{2+} (Figure 6A); consequently, 97% of the increase in J_o must be explained by an increase in the conductance of this pathway (L_{Oxphos}). The overall driving force for the ETC ($\Delta G_{NADH} - \Delta G_{\Delta\Psi}$) actually decreased by 15% with Ca^{2+} (Figure 6C), and, as a result, the increase in L_{ETC} is able to explain the entire Ca^{2+}- induced increase in flux down this pathway. Within the ETC, 100% and 98% of the greater flux observed with Ca^{2+} is explained by an increase in the conductances of Complex I+III (Figure 9A) and Complex IV (Figures 9C-D), respectively. Similarly, the driving force for the combined fuel transport and substrate dehydrogenase pathways ($\Delta G_{Fuel} - \Delta G_{NADH}$) decreased slightly with Ca^{2+}, suggesting that a change in conductance, and not driving force, is entirely responsible for the increase in flux observed with Ca^{2+}. Although the level of NADH and $\Delta\Psi$ merely reflect the balance of their respective production and utilization and do not offer direct insight into the specific location of any conductance changes, similar comparisons of the contribution of driving force versus conductance to the observed increase in flux can also be made for these two energetic intermediates. Ca^{2+} caused a 4% increase in both NADH and $\Delta\Psi$ (Figure 4); thus, the contribution of these two driving forces to the 2.01-fold increase in J_o was minimal compared to the associated increases in conductance due to Ca^{2+}.

Conversely, addition of Ca^{2+} led to an average 1.25-fold increase in $\Delta G_{\Delta\Psi} - \Delta G_{ATP}$ (Figure 6B), thus, only 76% of the increase in flux through the ATP production and transport reactions can be explained by L_{ATPase}. That ($\Delta G_{\Delta\Psi} - \Delta G_{ATP}$) was also able to explain a significant fraction of the Ca^{2+}-stimulated flux suggests that this thermodynamic parameter itself may play an important role in flux control. Similarly, the reduction level of cyt a_{607} (Figure 8e) is reported to be a primary controller of flux through Complex IV (67). Just as with ($\Delta G_{\Delta\Psi} - \Delta G_{ATP}$), the increase in reduction level of cyt a_{607} is able to explain 54% of the increase in flux through Complex IV due to Ca^{2+}, leaving 46% to be explained by activation of the enzyme. Moreover, in preliminary experiments where J_o was manipulated first by titrating increasing amounts of fuel (Push) and subsequently by increasing the PCr/Cr ratio (Pull), of the energetic parameters measured here, only ($\Delta G_{\Delta\Psi} - \Delta G_{ATP}$) and the reduction level of a_{607} maintained a positive, linear relationship with J_o during both the Push and Pull phases (Figures S1 and S2). Thus, these data suggest that ($\Delta G_{\Delta\Psi} - \Delta G_{ATP}$), the reduction level of cyt a_{607}, and the conductances through each step all play an important role in determining the rate of mitochondrial energy conversion.

Extrapolation to In Vivo Skeletal Muscle

The extrapolation of these data to *in vivo* conditions is complicated by the mitochondrial isolation process, the incubation conditions, and the removal from the local, cellular environment. However, these comparisons are useful in understanding these limitations. The addition of Ca^{2+} to levels similar to those observed during exercise *in vivo* provided a two-fold increase in the maximum velocity of mitochondrial energy conversion *in vitro* (Figure 3). Ca^{2+} has been proposed to play a significant role in the matching of energy supply with

demand in the heart (12, 81) where AT P turnover can increase five-fold with no change in the cellular energy level (82). Evidence for a balanced activation of the energy supply and demand pathways in skeletal muscle had been limited to *in silico* models (11, 76, 77) until recently when Wüst et al. (13) reported that the rapid rise in J_o observed at the onset of muscle contractions *in vivo* was best described by a model of 'parallel activation.' These authors showed that the increase in [ADP] at the onset of exercise was insufficient to account for the fast rise in J_o observed; instead, an increase in the apparent V_{max} of oxidative phosphorylation was required to explain their results. The [ADP] and K_m values reported for the canine gastrocnemius in the study by Wüst et al. (13) covered the range evaluated here (range: 17 – 66 μM, K_m: 43 μM), however, they reported ∼17-fold increase in J_o over this range of [ADP] *in vivo*, whereas we find a 4.2-fold increase in J_o with the combined effects of ADP and Ca^{2+} *in vitro* (Figure 3B). The lower dynamic range *in vitro* is also demonstrated by the respiratory control ratio of ∼15 (Table 1) when the *in vivo* values have been reported to approach 100 (1). The lower dynamic range of our measures could be due to a lower maximum rate of oxidative phosphorylation or due to a higher 'resting' rate. Combining the measured cytochrome a,a_3 content of 11.8 ± 1.6 nmol cyt a/g wet weight for the porcine vastus intermedius with the measured *in vitro* J_o at ∼66 μM ADP (259.2 nmol O_2/min/nmol cyt a) approaches the *in vivo* value reported by Wüst et al. (∼65 ml O_2/kg muscle/min) while at ∼17 μM ADP – Ca^{2+}, the rates were 15.2 ml O_2/kg muscle/min (*in vitro*) and 3.8 ml O_2/kg muscle/min (*in vivo*) suggesting that the maximum rate is similar under both conditions and that the discrepancy primarily resided in the resting rates (note that 'resting' here is defined as the 17 μM ADP, no Ca^{2+} condition). The reasons for this may be several-fold. First, in order to make simultaneous, quantitative measurements of J_o, NADH, and ΔΨ, we used isolated mitochondria removed from their native, reticular environment. Though these mitochondria were of high purity (21) and functional integrity, it is likely that the isolation process alters mitochondrial function to some degree (83). Indeed, PDH is reported to be activated after mitochondrial isolation (28, 84), and, together with other dehydrogenases, may contribute to a higher resting J_o *in vitro*. Similar results have been obtained for Complex IV and Complex V where heart biopsies had 2 – 4 fold lower activity compared to mitochondria isolated from the same tissue (49). Second, these studies were performed with an excess of glutamate and malate to ensure there would be no fuel limitations and to help maintain the steady state. This could result in a higher than normal delivery of reducing equivalents and also increase the 'resting' J_o. Finally, the leak rate may also be enhanced during the highly disruptive mitochondrial isolation process (83). Taking these points together, the combination of excess substrates, alterations in membrane leaks, and the activation of metabolic enzyme activity by the mitochondrial isolation process is likely to explain much of the increased 'resting' J_o *in vitro* compared to *in vivo*. However, the resultant lower J_o dynamic range *in vitro* would be expected to render the mitochondria less sensitive to Ca^{2+}; thus, the results presented here may actually underestimate the effect of Ca^{2+} *in vivo*. Indeed, simultaneous measures of mitochondrial ΔΨ, NADH, cytochrome redox state and phosphorylation potential in the intact functioning muscle should provide a better understanding of how the mechanisms outlined in isolated mitochondria may be in play *in vivo*.

Assumptions and Calculations

The nature of these experiments cannot distinguish between mitochondrial surface and matrix calcium effects. It was assumed that most of these effects are primarily due to changes in matrix calcium based on several factors. First, it has been shown that matrix Ca^{2+} rises *in vivo* with muscle contraction. Rogers et al. (85) demonstrated using Ca^{2+}- sensitive bioluminescence probes that the mitochondrial Ca^{2+} activity does increase with skeletal muscle contraction in an *in vivo* transgenic mouse. These data support the results of earlier, more invasive studies (86) and confirm the notion that an influx of Ca^{2+} into the mitochondrial matrix is occurring in the exercising muscle. Second, as reviewed by Glancy and Balaban (53), most of the effects on mitochondrial metabolism by Ca^{2+} are eliminated by blocking Ca^{2+} entry into the mitochondrial matrix. Extra-mitochondrial Ca^{2+} can impact some mitochondrial transporters, such as aralar (87) which, as part of the malate-aspartate shuttle (MAS), has been shown to play an important role in flux control in brain mitochondria (88). However, we believe there is little flux control by aralar in skeletal muscle mitochondria as aralar activity is five-fold higher in mitochondria from skeletal muscle compared to brain for any given [Ca^{2+}] (89). Thus, while Ca^{2+}-stimulation of aralar may remove a limitation to flux in brain mitochondria, the basal activity of aralar in skeletal muscle mitochondria is likely sufficient as to not impede flux. Moreover, in preliminary experiments, we gave mitochondria G+M and used arsenite to inhibit 2-oxoglutarate dehydrogenase, ensuring that only the mitochondrial components of the MAS were capable of providing NADH to the ETC and that aralar was the primary site of glutamate entry into the matrix. In these conditions, State 3 J_o was no different with and without Ca^{2+} and was similar to the No Ca^{2+} condition without arsenite present (data not shown). These results suggest that the two-fold activation of J_o with Ca^{2+} as shown in Figure 1 was largely through effects beyond those on aralar.

The calculation of the various ΔG values reported here requires a number of additional assumptions to be made. The first is the attainment of the fully oxidized and reduced states for each redox pair. For cytochromes c_1 and c, we used sodium hydrosulfite to reach full chemical reduction at the end of each experiment. However, we are unable to use this method with NADH because, in addition to the NADH fluorescent enhancement by binding to Complex I (90), the fluorescent signal is dependent on mitochondrial integrity and is severely disturbed by sodium hydrosulfite. As a result, fully reduced NADH was determined at anoxia and in the presence of Ca^{2+} for every experiment. The fully oxidized state for NADH and the cytochromes was determined after the 6-minute Ca^{2+} depletion and subsequent additions of 10 mM Pi and 0.13 mM ADP. Under this condition, the fluorescent NADH signal is ∼10% above that of the dark current even without correcting for non-NADH fluorescent background in the mitochondria, suggesting that NADH can only be further oxidized a maximum of ∼10%. This implied that the primary reducing equivalent source for the cytochromes was highly oxidized under these conditions, supporting our assumption that this was a reasonable estimate of the fully oxidized state of the “downstream” cytochromes. We were unable to measure full chemical (ferricyanide) oxidation in intact mitochondria due to the disruption of the mitochondrial structure with this agent.

The next step in the ΔG calculations involves calculating redox potentials (E_h) from % reduced values (Eq. 1) and requires a midpoint potential (E_m) for each redox pair. E_m values, especially for the various forms of cyt a as well as cyt c, are highly variable throughout the literature, and while the choice of E_m to use for each redox pair does alter the absolute ΔG values, the slopes in Figures 4, 6, 8, and 9 do not change regardless of the E_m chosen. Thus, the E_m values chosen have no effect on the relative conclusions made herein with regard to Ca^{2+}. The final assumptions made in the ΔG calculations are the values to use for the number of electrons transferred (n), the relative distance electrons travel across the width of the inner membrane between redox pairs (z), the number of protons pumped (m), and the P/O ratio (p) (Eqs. 3-5). All ΔG calculations were made assuming 1 NADH donated 2 electrons (n) yielding 10 protons (m) resulting in 2.7 ATP (p) from the consumption of $½O_2$. The pumping of 4, 4, and 2 protons per 2 electrons passed by Complexes I, III, and IV, respectively, has been widely accepted. Further validation of the values chosen for n, m, and z and the E_m values is provided by the measurement of force ratios (40-42) which provides the value for the number of protons pumped per electron transferred under equilibrium, or static head, conditions. Table 4 shows the close matching between the theoretical and measured stoichiometry values used in the free energy calculations, and perhaps more importantly, that there was no difference with the addition of Ca^{2+}.

The number of protons required to elicit a 360° rotation of the γ subunit of Complex V and synthesize 3 ATP is thought to be determined by the size of the c ring within Complex V (91). Mammalian Complex V has 8 c subunits (92), thus H/ATP is 8/3 or 2.67. However, transport of ATP out of the mitochondria also comes at the expense of one proton, thus, the overall H/ATP is 3.67 yielding a P/O ratio of 10/3.67 or 2.7. This value represents the theoretical maximal P/O ratio, as the actual value may be lower due to contribution of the proton leak. Unfortunately, we did not measure proton leak kinetics here; however, based on the respiratory control ratios reported in Table 1, the contribution of the proton leak in these mitochondria under phosphorylating conditions is likely very low. By assuming that proton leak is 100% of State 4 respiration and zero at State 3 and utilizing a standard relationship between membrane potential and proton leak, we can estimate that accounting for the proton leak would alter the slopes in Figure 6B by ∼10% and have a less than 5% effect on the No Ca^{2+}/Ca^{2+} ratio between slopes. Further, we do not expect a difference in proton leak between Ca^{2+} and No Ca^{2+} conditions as Ca^{2+} doesn't alter proton leak kinetics in either heart (80) or skeletal muscle mitochondria (6) oxidizing NAD-linked substrates and we find no difference in ADP/O with Ca^{2+} in heart mitochondria (9).

Additionally, we did not attempt to measure the contribution of the pH gradient to the protonmotive force in this study. Lambert and Brand (25) found that increasing [Pi] lowered the pH gradient in skeletal muscle mitochondria, and extrapolation of their data to 10 mM Pi as used here would make the pH gradient nearly zero. Moreover, the use of 15 mM sodium in our medium, and the resultant sodium/proton exchange, would be expected to drive the pH gradient even lower than that observed by Lambert and Brand (25). In addition, we previously reported that there was no pH gradient in phosphorylating mitochondria under similar conditions to those used in this study (23). Finally, Kavanagh et al. (6) reported that the pH gradient did not change across a wide range of respiration rates in skeletal muscle mitochondria given NAD-linked substrates with and without Ca^{2+}. Thus, any contribution of

the pH gradient could be expected to be the same for all points in the force:flow plots, thereby yielding no effect on the slopes and, therefore, the results reported here.

Initial free energy analyses involving cyt a were done similarly to those mentioned above where sodium hydrosulfite was used to determine the fully reduced state using the spectral peak observed at 605 nm, redox potential was determined using a published E_m value, ΔG was calculated using the appropriate proton and electron stoichiometries, and these assumptions were validated by the measurement of the force ratios (Table 4). However, as discussed in previous work (31), closer examination revealed that the spectral peak for cyt a in the presence of oxygen was consistently observed at 607 nm and not 605 nm, suggesting that the detected species was the peroxy form of cyt a_3 (31, 32). The peroxy form of cyt a_3 is just one of several intermediates within the catalytic cycle of Complex IV and is not present in both oxidized and reduced forms as with the b and c cytochromes. Further complicating matters, maximum occupancy of a_{607} has been reported to represent only ∼30% of the total enzyme (93, 94), suggesting that most of the enzyme complex is in different redox states. These findings bring into question the validity of the assumptions made in the quantification of $\Delta G_{cyt\ a607}$ discussed above. It should be noted that the determination of cyt a content in detergent extracts with chemical reducing agents does not suffer from this complication since the entire Complex is moved to the fully reduced state. Fortunately, we can use the measurements of L_{ETC} and $L_{CI+CIII}$ to subtract the conductance of Complex I+III from the conductance of the entire ETC to yield another measurement of the conductance of Complex IV. Using this calculation, Ca^{2+} still provides a more than two-fold increase in the conductance of Complex IV, and the subsequent calculation of resistances as in Table 3 suggests that Complex IV is still the primary site of resistance in the absence of Ca^{2+} and that the relative resistance is reduced upon the addition of Ca^{2+} (data not shown). Additionally, calculation of the conductance of Complex IV can be done by combining L_{CIVa} and L_{CIVb} and plotting ($\Delta G_{cyt\ c\ –\ O2/H2O}$ - $\Delta G_{\Delta\Psi}$) versus J_o. Again, this calculation provides similar results with regard to the effect of Ca^{2+} on the conductance of Complex IV and its resistance relative to the entire energy conversion cascade. These two calculations, combined with the validity provided by the force ratio measurements, suggest that the interpretations resultant from the initial analyses on the effect of Ca^{2+} on Complex IV were justified. Moreover, we performed additional analyses on the conductance of electron transfer within Complex IV using a method similar to Wikström and Morgan (32) where the peroxy and ferryl forms of cyt a were considered one redox couple and the ferryl and oxidized forms were considered another. These results are displayed in Figure 10 and further suggest that Ca^{2+} activates Complex IV by altering the conductance of electron transfer within the catalytic cycle of the enzyme in addition to reducing the contribution of Complex IV to the overall resistance to energy conversion.

Ca^{2+} has also been shown to induce a spectral shift in heme a of Complex IV (95, 96), and it is possible that this confounded our results with respect to the Ca^{2+} activation of Complex IV depicted in Figures 9 and 10. To investigate this possibility, we repeated the experiments of Kirichenko et al. (95) using solubilized porcine mitochondria where cyt a was reduced by KCN, ascorbate, and TMPD. Indeed, addition of Ca^{2+} induced a red shift of cyt a (data not shown). However, the addition of Ca^{2+} to intact, respiring mitochondria where Complex IV

is more than 90% oxidized induced no such shift in the peak for cyt a suggesting that the observed Ca^{2+} activation of Complex IV is not simply due to a Ca^{2+}-induced spectral shift.

Summary

These data present the first experimental evidence of a systemic modulation of the oxidative phosphorylation cascade by Ca^{2+}. This stimulation involves the near balanced activation of the entire mitochondrial energy conversion process from the generation of NADH and reduction of oxygen to the formation of ATP from ADP and Pi. While the mechanism explaining this systemic modulation with Ca^{2+} has yet to be elucidated, current evidence suggests that it is not direct Ca^{2+} binding as studies on isolated membrane enzymes and submitochondrial particles find no effect of Ca^{2+} (61, 97). Thus, it seems likely that Ca^{2+} is acting through an as yet unknown coordination of post-translational modifications (PTMs). Whether this involves alterations in supercomplex structure (98), changes in phosphorylation, multiple PTMs, or other possibilities will be the subject of future work. Additionally, extrapolation of these data to the conditions observed during exercise in skeletal muscle *in vivo* reveals that a significant fraction of the metabolic activation associated with exercise could be attributed to Ca^{2+} effects on oxidative phosphorylation coupled with an increase in [ADP], thereby contributing to the metabolic homeostasis of this dynamic tissue.

Supplementary Material

Refer to Web version on PubMed Central for supplementary material.

Acknowledgments

Funding Source: This study was supported by Intramural Funding of the Division of Intramural Research, National Heart, Lung, and Blood Institute.

References

1. Weibel ER, Hoppeler H. Exercise-induced maximal metabolic rate scales with muscle aerobic capacity. J Exp Biol. 2005; 208:1635–1644. [PubMed: 15855395]
2. Combs CA, Aletras AH, Balaban RS. Effect of muscle action and metabolic strain on oxidative metabolic responses in human skeletal muscle. J Appl Physiol. 1999; 87:1768–1775. [PubMed: 10562621]
3. Connett R, Honig C. Regulation of VO_2 in red muscle: do current biochemical hypotheses fit in vivo data. Am J Physiol. 1989; 256:R898–R906. [PubMed: 2705578]
4. Kushmerick M, Meyer R, Brown T. Regulation of oxygen consumption in fast- and slow twitch muscle. Am J Physiol. 1992; 263:C598–C606. [PubMed: 1415510]
5. Johnston JD, Brand MD. Stimulation of the respiration rate of rat liver mitochondria by sub-micromolar concentrations of extramitochondrial Ca2+ Biochem J. 1987; 245:217–222. [PubMed: 3663147]
6. Kavanagh NI, Ainscow EK, Brand MD. Calcium regulation of oxidative phosphorylation in rat skeletal muscle mitochondria. Biochim Biophys Acta. 2000; 1457:57–70. [PubMed: 10692550]
7. McCormack JG, Halestrap AP, Denton RM. Role of calcium ions in regulation of mammalian intramitochondrial metabolism. Physiol Rev. 1990; 70:391–425. [PubMed: 2157230]
8. Panov AV, Scaduto RC Jr. Substrate specific effects of calcium on metabolism of rat heart mitochondria. Am J Physiol. 1996; 270:H1398–1406. [PubMed: 8967382]

9. Territo PR, Mootha VK, French SA, Balaban RS. Ca(2+) activation of heart mitochondrial oxidative phosphorylation: role of the F(0)/F(1)-ATPase. Am J Physiol Cell Physiol. 2000; 278:C423–435. [PubMed: 10666039]
10. Balaban RS. Regulation of oxidative phosphorylation in the mammalian cell. Am J Physiol. 1990; 258:C377–389. [PubMed: 2138418]
11. Korzeniewski B. Regulation of oxidative phosphorylation through parallel activation. Biophys Chem. 2007; 129:93–110. [PubMed: 17566629]
12. Balaban RS, Bose S, French SA, Territo PR. Role of calcium in metabolic signaling between cardiac sarcoplasmic reticulum and mitochondria in vitro. Am J Physiol Cell Physiol. 2003; 284:C285–293. [PubMed: 12529248]
13. Wust RC, Grassi B, Hogan MC, Howlett RA, Gladden LB, Rossiter HB. Kinetic control of oxygen consumption during contractions in self-perfused skeletal muscle. J Physiol. 2011; 589:3995–4009. [PubMed: 21690197]
14. McCormack JG, Denton RM. Role of calcium ions in the regulation of intramitochondrial metabolism. Properties of the Ca2+-sensitive dehydrogenases within intact uncoupled mitochondria from the white and brown adipose tissue of the rat. Biochem J. 1980; 190:95–105. [PubMed: 6778477]
15. Murphy AN, Kelleher JK, Fiskum G. Submicromolar Ca2+ regulates phosphorylating respiration by normal rat liver and AS-30D hepatoma mitochondria by different mechanisms. J Biol Chem. 1990; 265:10527–10534. [PubMed: 2113059]
16. Martin C, Dubouchaud H, Mosoni L, Chardigny JM, Oudot A, Fontaine E, Vergely C, Keriel C, Rochette L, Leverve X, Demaison L. Abnormalities of mitochondrial functioning can partly explain the metabolic disorders encountered in sarcopenic gastrocnemius. Aging cell. 2007; 6:165–177. [PubMed: 17286611]
17. Carroll SL, Klein MG, Schneider MF. Decay of calcium transients after electrical stimulation in rat fast- and slow-twitch skeletal muscle fibres. J Physiol. 1997; 501:573–588. [PubMed: 9218218]
18. Westerblad H, Allen DG. Changes of myoplasmic calcium concentration during fatigue in single mouse muscle fibers. J Gen Physiol. 1991; 98:615–635. [PubMed: 1761971]
19. Westerblad H, Duty S, Allen DG. Intracellular calcium concentration during low-frequency fatigue in isolated single fibers of mouse skeletal muscle. J Appl Physiol. 1993; 75:382–388. [PubMed: 8397180]
20. Moreno-Sanchez R, Hogue BA, Hansford RG. Influence of NAD-linked dehydrogenase activity on flux through oxidative phosphorylation. Biochem J. 1990; 268:421–428. [PubMed: 2363681]
21. Glancy B, Balaban RS. Protein composition and function of red and white skeletal muscle mitochondria. Am J Physiol Cell Physiol. 2011; 300:C1280–1290. [PubMed: 21289287]
22. Balaban RS, Mootha VK, Arai A. Spectroscopic determination of cytochrome c oxidase content in tissues containing myoglobin or hemoglobin. Anal Biochem. 1996; 237:274–278. [PubMed: 8660576]
23. Bose S, French S, Evans FJ, Joubert F, Balaban RS. Metabolic network control of oxidative phosphorylation: multiple roles of inorganic phosphate. J Biol Chem. 2003; 278:39155–39165. [PubMed: 12871940]
24. Rasmussen HN, Rasmussen UF. Oxygen solubilities of media used in electrochemical respiration measurements. Anal Biochem. 2003; 319:105–113. [PubMed: 12842113]
25. Lambert AJ, Brand MD. Superoxide production by NADH:ubiquinone oxidoreductase (complex I) depends on the pH gradient across the mitochondrial inner membrane. Biochem J. 2004; 382:511–517. [PubMed: 15175007]
26. Fabiato A, Fabiato F. Calculator programs for computing the composition of the solutions containing multiple metals and ligands used for experiments in skinned muscle cells. J Physiol (Paris). 1979; 75:463–505. [PubMed: 533865]
27. Reitz FB, Pollack GH. Labview virtual instruments for calcium buffer calculations. Comput Methods Programs Biomed. 2003; 70:61–69. [PubMed: 12468127]
28. Messer JI, Jackman MR, Willis WT. Pyruvate and citric acid cycle carbon requirements in isolated skeletal muscle mitochondria. Am J Physiol Cell Physiol. 2004; 286:C565–572. [PubMed: 14602577]

29. Lefort N, Glancy B, Bowen B, Willis WT, Bailowitz Z, De Filippis EA, Brophy C, Meyer C, Hojlund K, Yi Z, Mandarino LJ. Increased reactive oxygen species production and lower abundance of complex I subunits and carnitine palmitoyltransferase 1B protein despite normal mitochondrial respiration in insulin-resistant human skeletal muscle. Diabetes. 2010; 59:2444–2452. [PubMed: 20682693]
30. Teague WE Jr, Dobson GP. Effect of temperature on the creatine kinase equilibrium. J Biol Chem. 1992; 267:14084–14093. [PubMed: 1629208]
31. Chess D, Billings E, Covian R, Glancy B, French S, Taylor J, Murphy E, Balaban RS. Optical spectroscopy of mitochondrial oxidative phosphorylation complexes using an integrating sphere: analysis of steady state reducing equivalent distributions, (submitted). 2012
32. Wikstrom M, Morgan JE. The dioxygen cycle. Spectral, kinetic, and thermodynamic characteristics of ferryl and peroxy intermediates observed by reversal of the cytochrome oxidase reaction. J Biol Chem. 1992; 267:10266–10273. [PubMed: 1316895]
33. Proshlyakov DA, Pressler MA, Babcock GT. Dioxygen activation and bond cleavage by mixed-valence cytochrome c oxidase. Proc Natl Acad Sci U S A. 1998; 95:8020–8025. [PubMed: 9653133]
34. Wikstrom M, Verkhovsky MI. Mechanism and energetics of proton translocation by the respiratory heme-copper oxidases. Biochim Biophys Acta. 2007; 1767:1200–1214. [PubMed: 17689487]
35. Kim YC, Wikstrom M, Hummer G. Kinetic gating of the proton pump in cytochrome c oxidase. Proc Natl Acad Sci U S A. 2009; 106:13707–13712. [PubMed: 19666617]
36. Tiesjema RH, Muijsers AO, van Gelder BF. Biochemical and biophysical studies on cytochrome c oxidase. X. Spectral and potentiometric properties of the hemes and coppers. Biochim Biophys Acta. 1973; 305:19–28. [PubMed: 4352553]
37. Muijsers AO, Tiesjema RH, Henderson RW, Van Gelder BF. Biochemical and biophysical studies on cytochrome aa 3 . VII. The effect of cytochrome c on the oxidation-reduction potential of isolated cytochrome aa 3. Biochim Biophys Acta. 1972; 267:216–221. [PubMed: 4336312]
38. Onsager L. Reciprocal relations in irreversible processes. II. Phys Rev. 1931; 38:2265–2279.
39. Onsager L. Reciprocal relations in irreversible processes. I. Phys Rev. 1931; 37:405–426.
40. Brown GC, Brand MD. Thermodynamic control of electron flux through mitochondrial cytochrome bc1 complex. Biochem J. 1985; 225:399–405. [PubMed: 2983670]
41. Brown GC, Brand MD. Proton/electron stoichiometry of mitochondrial complex I estimated from the equilibrium thermodynamic force ratio. Biochem J. 1988; 252:473–479. [PubMed: 2843170]
42. Lemasters JJ. The ATP-to-oxygen stoichiometries of oxidative phosphorylation by rat liver mitochondria. An analysis of ADP-induced oxygen jumps by linear nonequilibrium thermodynamics. J Biol Chem. 1984; 259:13123–13130. [PubMed: 6548475]
43. Hughes BP, Barritt GJ. Effects of glucagon and N6O2′- dibutyryladenosine 3′:5′-cyclic monophosphate on calcium transport in isolated rat liver mitochondria. Biochem J. 1978; 176:295–304. [PubMed: 215132]
44. Carafoli E, Lehninger AL. A survey of the interaction of calcium ions with mitochondria from different tissues and species. Biochem J. 1971; 122:681–690. [PubMed: 5129264]
45. Territo PR, French SA, Dunleavy MC, Evans FJ, Balaban RS. Calcium activation of heart mitochondrial oxidative phosphorylation: rapid kinetics of mVO2, NADH, AND light scattering. J Biol Chem. 2001; 276:2586–2599. [PubMed: 11029457]
46. Glancy B, Barstow T, Willis WT. Linear relation between time constant of oxygen uptake kinetics, total creatine, and mitochondrial content in vitro. Am J Physiol Cell Physiol. 2008; 294:C79–87. [PubMed: 17942641]
47. Kushmerick MJ, Meyer RA, Brown TR. Regulation of oxygen consumption in fast- and slow-twitch muscle. Am J Physiol. 1992; 263:C598–606. [PubMed: 1415510]
48. Ryschon TW, Fowler MD, Wysong RE, Anthony A, Balaban RS. Efficiency of human skeletal muscle in vivo: comparison of isometric, concentric, and eccentric muscle action. J Appl Physiol. 1997; 83:867–874. [PubMed: 9292475]
49. Phillips D, Covian R, Aponte AM, Glancy B, Taylor JF, Chess D, Balaban RS. Regulation of oxidative phosphorylation complex activity: effects of tissue-specific metabolic stress within an

allometric series and acute changes in workload. Am J Physiol Regul Integr Comp Physiol. 2012; 302:R1034–1048. [PubMed: 22378775]

50. Turner PR, Westwood T, Regen CM, Steinhardt RA. Increased protein degradation results from elevated free calcium levels found in muscle from mdx mice. Nature. 1988; 335:735–738. [PubMed: 3173492]
51. Jones AM, Wilkerson DP, Fulford J. Influence of dietary creatine supplementation on muscle phosphocreatine kinetics during knee-extensor exercise in humans. American Journal of Physiology-Regulatory Integrative and Comparative Physiology. 2009; 296:R1078–R1087.
52. Kemp GJ, Taylor DJ, Radda GK. Control of phosphocreatine resynthesis during recovery from exercise in human skeletal muscle. NMR in biomedicine. 1993; 6:66–72. [PubMed: 8457428]
53. Glancy B, Balaban RS. Role of mitochondrial Ca2+ in the regulation of cellular energetics. Biochemistry. 2012; 51:2959–2973. [PubMed: 22443365]
54. Starkov AA, Fiskum G. Regulation of brain mitochondrial H2O2 production by membrane potential and NAD(P)H redox state. J Neurochem. 2003; 86:1101–1107. [PubMed: 12911618]
55. Hopper RK, Carroll S, Aponte AM, Johnson DT, French S, Shen RF, Witzmann FA, Harris RA, Balaban RS. Mitochondrial matrix phosphoproteome: effect of extra mitochondrial calcium. Biochemistry. 2006; 45:2524–2536. [PubMed: 16489745]
56. Brookes PS, Yoon Y, Robotham JL, Anders MW, Sheu SS. Calcium, ATP, and ROS: a mitochondrial love-hate triangle. Am J Physiol Cell Physiol. 2004; 287:C817–833. [PubMed: 15355853]
57. Starkov AA, Polster BM, Fiskum G. Regulation of hydrogen peroxide production by brain mitochondria by calcium and Bax. J Neurochem. 2002; 83:220–228. [PubMed: 12358746]
58. Covian R, Trumpower BL. The dimeric structure of the cytochrome bc(1) complex prevents center P inhibition by reverse reactions at center N. Biochim Biophys Acta. 2008; 1777:1044–1052. [PubMed: 18454936]
59. Covian R, Zwicker K, Rotsaert FA, Trumpower BL. Asymmetric and redox-specific binding of quinone and quinol at center N of the dimeric yeast cytochrome bc1 complex. Consequences for semiquinone stabilization. J Biol Chem. 2007; 282:24198–24208. [PubMed: 17584742]
60. Kim N, Ripple MO, Springett R. Measurement of the mitochondrial membrane potential and pH gradient from the redox poise of the hemes of the bc1 complex. Biophys J. 2012; 102:1194–1203. [PubMed: 22404942]
61. Bender E, Kadenbach B. The allosteric ATP-inhibition of cytochrome c oxidase activity is reversibly switched on by cAMP-dependent phosphorylation. FEBS Lett. 2000; 466:130–134. [PubMed: 10648827]
62. Gandra PG, Nogueira L, Hogan MC. Mitochondrial activation at the onset of contractions in isolated myofibres during successive contractile periods. J Physiol. 2012; 590:3597–3609. [PubMed: 22711953]
63. Kummel A, Panke S, Heinemann M. Systematic assignment of thermodynamic constraints in metabolic network models. BMC Bioinformatics. 2006; 7:512. [PubMed: 17123434]
64. Oster GF, Perelson AS, Katchalsky A. Network thermodynamics: dynamic modelling of biophysical systems. Q Rev Biophys. 1973; 6:1–134. [PubMed: 4576440]
65. Wan B, LaNoue KF, Cheung JY, Scaduto RC Jr. Regulation of citric acid cycle by calcium. J Biol Chem. 1989; 264:13430–13439. [PubMed: 2503501]
66. Harris D, Das A. Control of mitochondrial ATP synthesis in the heart. Biochem J. 1991; 280:561–573. [PubMed: 1837214]
67. Wilson DF, Owen CS, Holian A. Control of mitochondrial respiration: a quantitative evaluation of the roles of cytochrome c and oxygen. Arch Biochem Biophys. 1977; 182:749–762. [PubMed: 20061]
68. Kholodenko B, Zilinskiene V, Borutaite V, Ivanoviene L, Toleikis A, Praskevicius A. The role of adenine nucleotide translocators in regulation of oxidative phosphorylation in heart mitochondria. FEBS Lett. 1987; 223:247–250. [PubMed: 2822484]
69. Korzeniewski B, Mazat JP. Theoretical studies on the control of oxidative phosphorylation in muscle mitochondria: application to mitochondrial deficiencies. Biochem J. 1996; 319(Pt 1):143–148. [PubMed: 8870661]

70. Davis E, Davis Van-Thienen W. Rate control of phosphorylation-coupled respiration by rat liver mitochondria. Arch Biochem Biophys. 1984; 233:573–581. [PubMed: 6486800]
71. Kacser H, Burns JA. The control of flux. Symp Soc Exp Biol. 1973; 27:65–104. [PubMed: 4148886]
72. Groen AK, Wanders RJ, Westerhoff HV, van der Meer R, Tager JM. Quantification of the contribution of various steps to the control of mitochondrial respiration. J Biol Chem. 1982; 257:2754–2757. [PubMed: 7061448]
73. Tager JM, Groen AK, Wanders RJ, Duszynski J, Westerhoff HV, Vervoorn RC. Control of mitochondrial respiration. Biochem Soc Trans. 1983; 11:40–43. [PubMed: 6298025]
74. Rossignol R, Letellier T, Malgat M, Rocher C, Mazat JP. Tissue variation in the control of oxidative phosphorylation: implication for mitochondrial diseases. Biochem J. 2000; 347(Pt 1):45–53. [PubMed: 10727400]
75. Fell DA, Thomas S. Physiological control of metabolic flux: the requirement for multisite modulation. Biochem J. 1995; 311(Pt 1):35–39. [PubMed: 7575476]
76. Korzeniewski B. Regulation of ATP supply during muscle contraction: theoretical studies. Biochem J. 1998; 330(Pt 3):1189–1195. [PubMed: 9494084]
77. Korzeniewski B. Regulation of ATP supply in mammalian skeletal muscle during resting state-->intensive work transition. Biophys Chem. 2000; 83:19–34. [PubMed: 10631477]
78. Hochachka PW, Matheson GO. Regulating ATP turnover rates over broad dynamic work ranges in skeletal muscles. J Appl Physiol. 1992; 73:1697–1703. [PubMed: 1474039]
79. Hagg SA, Taylor SI, Ruberman NB. Glucose metabolism in perfused skeletal muscle. Pyruvate dehydrogenase activity in starvation, diabetes and exercise. Biochem J. 1976; 158:203–210. [PubMed: 825112]
80. Mildaziene V, Baniene R, Nauciene Z, Marcinkeviciute A, Morkuniene R, Borutaite V, Kholodenko B, Brown GC. Ca2+ stimulates both the respiratory and phosphorylation subsystems in rat heart mitochondria. Biochem J. 1996; 320(Pt 1):329–334. [PubMed: 8947505]
81. Balaban RS. Cardiac energy metabolism homeostasis: role of cytosolic calcium. J Mol Cell Cardiol. 2002; 34:1259–1271. [PubMed: 12392982]
82. Balaban RS, Kantor HL, Katz LA, Briggs RW. Relation between work and phosphate metabolite in the in vivo paced mammalian heart. Science. 1986; 232:1121–1123. [PubMed: 3704638]
83. Picard M, Taivassalo T, Ritchie D, Wright KJ, Thomas MM, Romestaing C, Hepple RT. Mitochondrial structure and function are disrupted by standard isolation methods. PLoS ONE. 2011; 6:e18317. [PubMed: 21512578]
84. Kerbey AL, Randle PJ, Cooper RH, Whitehouse S, Pask HT, Denton RM. Regulation of pyruvate dehydrogenase in rat heart. Mechanism of regulation of proportions of dephosphorylated and phosphorylated enzyme by oxidation of fatty acids and ketone bodies and of effects of diabetes: role of coenzyme A, acetyl-coenzyme A and reduced and oxidized nicotinamide-adenine dinucleotide. Biochem J. 1976; 154:327–348. [PubMed: 180974]
85. Rogers KL, Picaud S, Roncali E, Boisgard R, Colasante C, Stinnakre J, Tavitian B, Brulet P. Non-invasive in vivo imaging of calcium signaling in mice. PLoS ONE. 2007; 2:e974. [PubMed: 17912353]
86. Rudolf R, Mongillo M, Magalhaes PJ, Pozzan T. In vivo monitoring of Ca(2+) uptake into mitochondria of mouse skeletal muscle during contraction. J Cell Biol. 2004; 166:527–536. [PubMed: 15314066]
87. Satrustegui J, Pardo B, Del Arco A. Mitochondrial transporters as novel targets for intracellular calcium signaling. Physiol Rev. 2007; 87:29–67. [PubMed: 17237342]
88. Gellerich FN, Gizatullina Z, Trumbekaite S, Korzeniewski B, Gaynutdinov T, Seppet E, Vielhaber S, Heinze HJ, Striggow F. Cytosolic Ca2+ regulates the energization of isolated brain mitochondria by formation of pyruvate through the malate-aspartate shuttle. Biochem J. 2012; 443:747–755. [PubMed: 22295911]
89. Contreras L, Gomez-Puertas P, Iijima M, Kobayashi K, Saheki T, Satrustegui J. Ca2+ Activation kinetics of the two aspartate-glutamate mitochondrial carriers, aralar and citrin: role in the heart malate-aspartate NADH shuttle. J Biol Chem. 2007; 282:7098–7106. [PubMed: 17213189]

90. Blinova K, Levine RL, Boja ES, Griffiths GL, Shi ZD, Ruddy B, Balaban RS. Mitochondrial NADH fluorescence is enhanced by complex I binding. Biochemistry. 2008; 47:9636–9645. [PubMed: 18702505]
91. Ferguson SJ. ATP synthase: from sequence to ring size to the P/O ratio. Proc Natl Acad Sci U S A. 2010; 107:16755–16756. [PubMed: 20858734]
92. Watt IN, Montgomery MG, Runswick MJ, Leslie AG, Walker JE. Bioenergetic cost of making an adenosine triphosphate molecule in animal mitochondria. Proc Natl Acad Sci U S A. 2010; 107:16823–16827. [PubMed: 20847295]
93. Proshlyakov DA, Ogura T, Shinzawa-Itoh K, Yoshikawa S, Appelman EH, Kitagawa T. Selective resonance Raman observation of the “607 nm” form generated in the reaction of oxidized cytochrome c oxidase with hydrogen peroxide. J Biol Chem. 1994; 269:29385–29388. [PubMed: 7961916]
94. Proshlyakov DA, Ogura T, Shinzawa-Itoh K, Yoshikawa S, Kitagawa T. Microcirculating system for simultaneous determination of Raman and absorption spectra of enzymatic reaction intermediates and its application to the reaction of cytochrome c oxidase with hydrogen peroxide. Biochemistry. 1996; 35:76–82. [PubMed: 8555201]
95. Kirichenko A, Vygodina T, Mkrtchyan HM, Konstantinov A. Specific cation binding site in mammalian cytochrome oxidase. FEBS Lett. 1998; 423:329–333. [PubMed: 9515733]
96. Wikstrom M, Saari H. A spectral shift in cytochrome a induced by calcium ions. Biochim Biophys Acta. 1975; 408:170–179. [PubMed: 811258]
97. Panov AV, Scaduto RC Jr. Influence of calcium on NADH and succinate oxidation by rat heart submitochondrial particles. Arch Biochem Biophys. 1995; 316:815–820. [PubMed: 7864638]
98. Lenaz G, Genova ML. Structural and functional organization of the mitochondrial respiratory chain: a dynamic super-assembly. Int J Biochem Cell Biol. 2009; 41:1750–1772. [PubMed: 19711505]

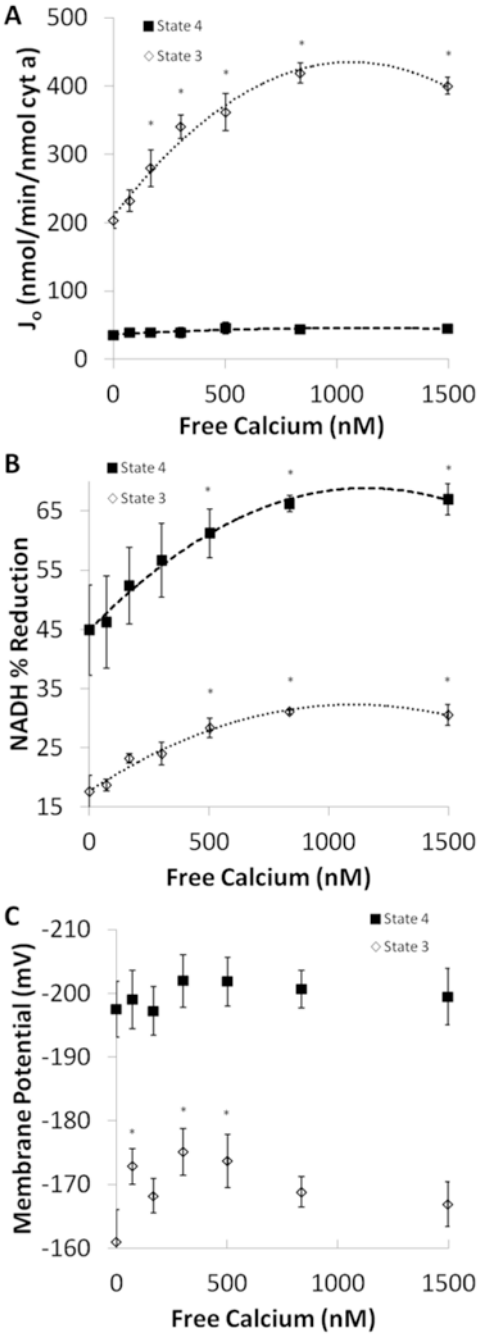

Figure 1.

Calcium titration. A: State 3 and 4 J_o at added free calcium concentrations from 0 to 1500 nM. B: State 3 and 4 NADH at added free calcium concentrations from 0 to 1500 nM. C: State 3 and 4 $\Delta\Psi$ at added free calcium concentrations from 0 to 1500 nM. Filled squares – State 4, open diamonds – State 3. Error bars signify standard error. * denotes significance difference from no calcium condition. n = 4.

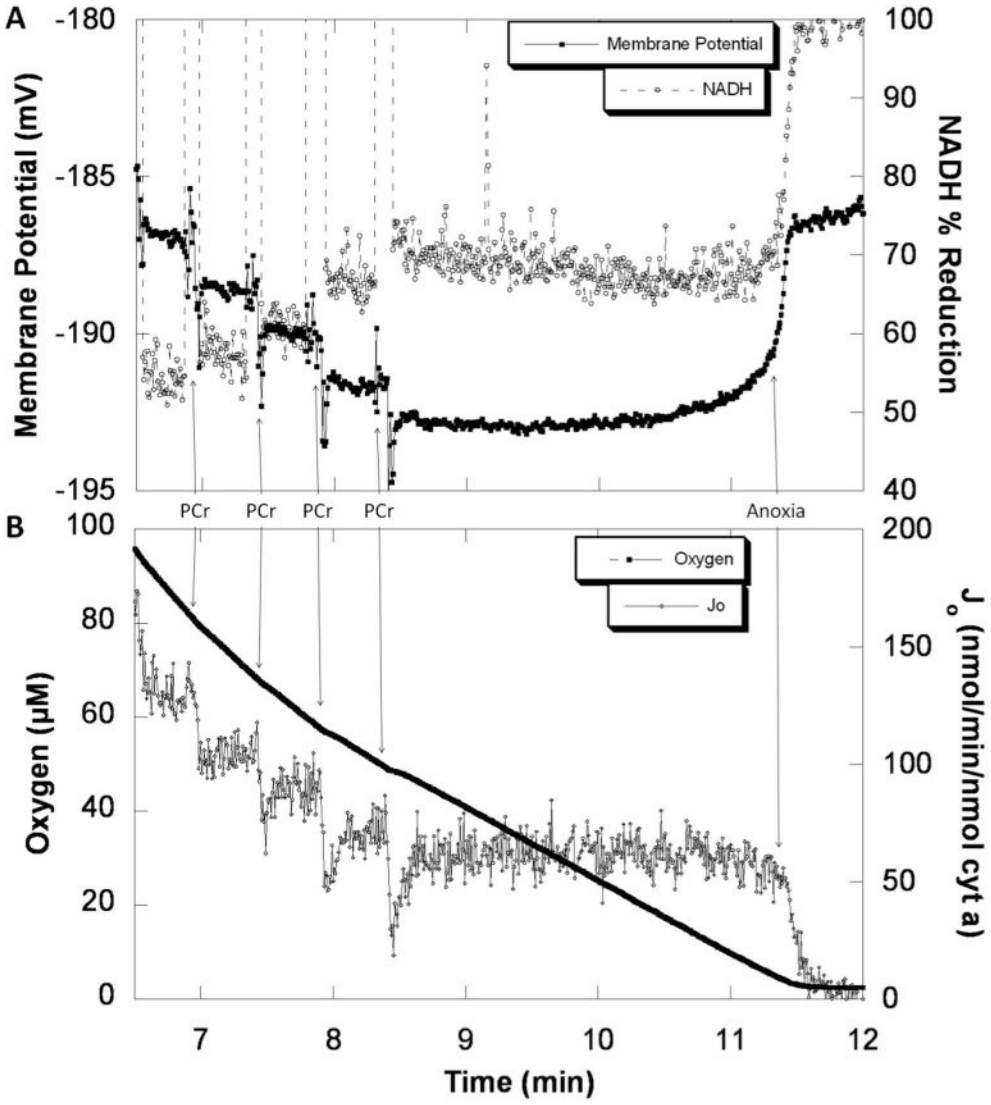

Figure 2.

Representative CK energetic clamp experiment. A: ΔΨ and NADH during stepwise PCr additions and at anoxia. B: J_o and $[O_2]$ during stepwise PCr additions and at anoxia.

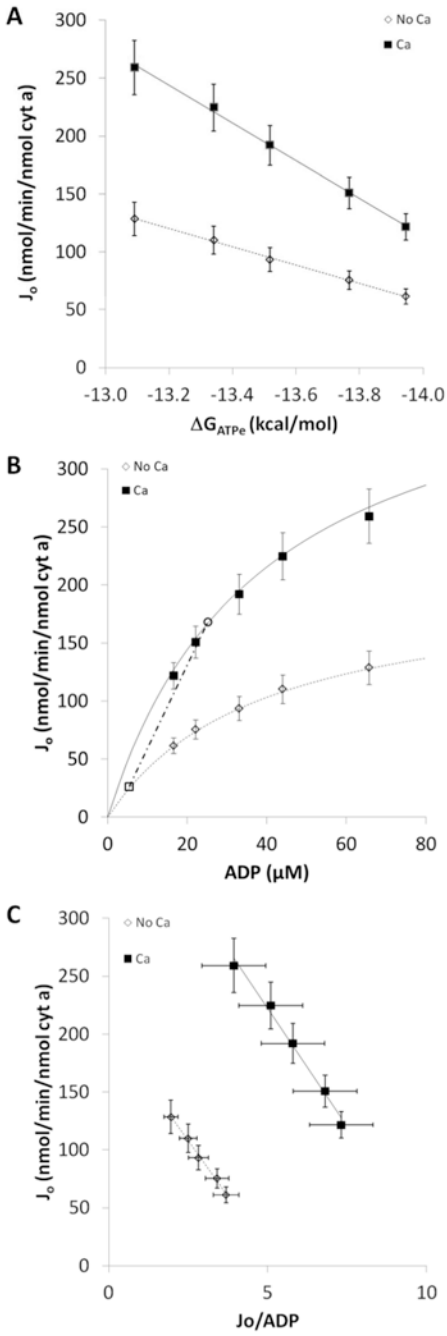

Figure 3.

Kinetic effect of calcium on oxidative phosphorylation intermediate respiration. A: Relationship between ΔG_{ATPe} and J_o with and without calcium. B: Michaelis-Menten relationship between J_o and ADP with and without calcium. The open square and open circle signify the ADP values reported for human skeletal muscle at rest and during moderate exercise, respectively. C: Eadie-Hofstee plot for the relationship between J_o and ADP where $y= -(K_mADP)x + V_{max}$. Filled squares – calcium, open diamonds – no calcium. Error bars

signify standard error. n = 12. Slopes, regression analyses, and the resultant p-values for A and C are reported in Table 2 under ΔG_{ATPe} and K_{mADP}, respectively.

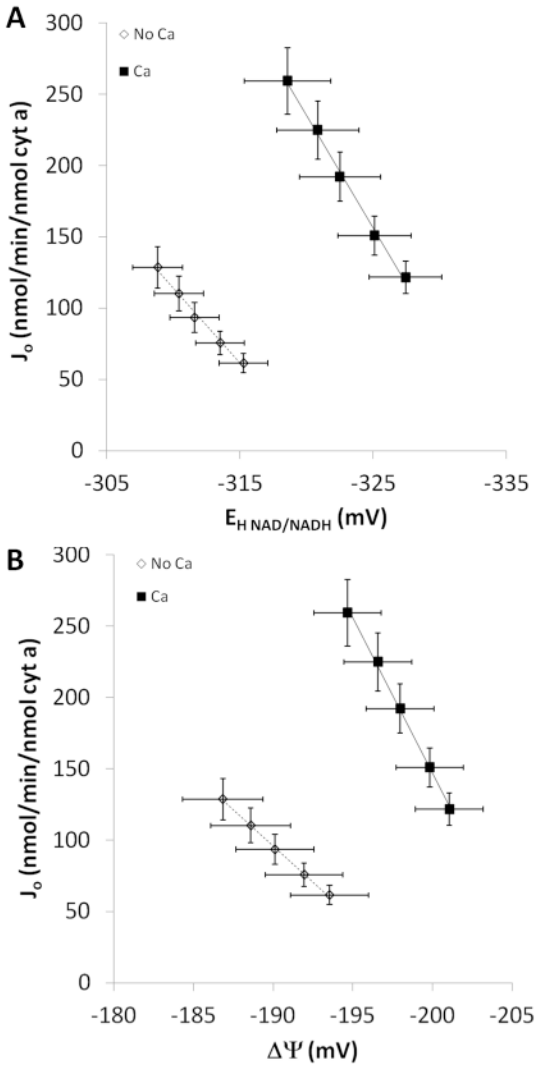

Figure 4.

Effect of calcium on oxidative phosphorylation energetic driving forces and J_o during intermediate respiration. A: Relationship between NADH and J_o with and without calcium. B: Relationship between ΔΨ and J_o with and without calcium. Filled squares – calcium, open diamonds – no calcium. Error bars signify standard error. n = 12. Slopes, regression analyses, and the resultant p-values are reported in Table 2.

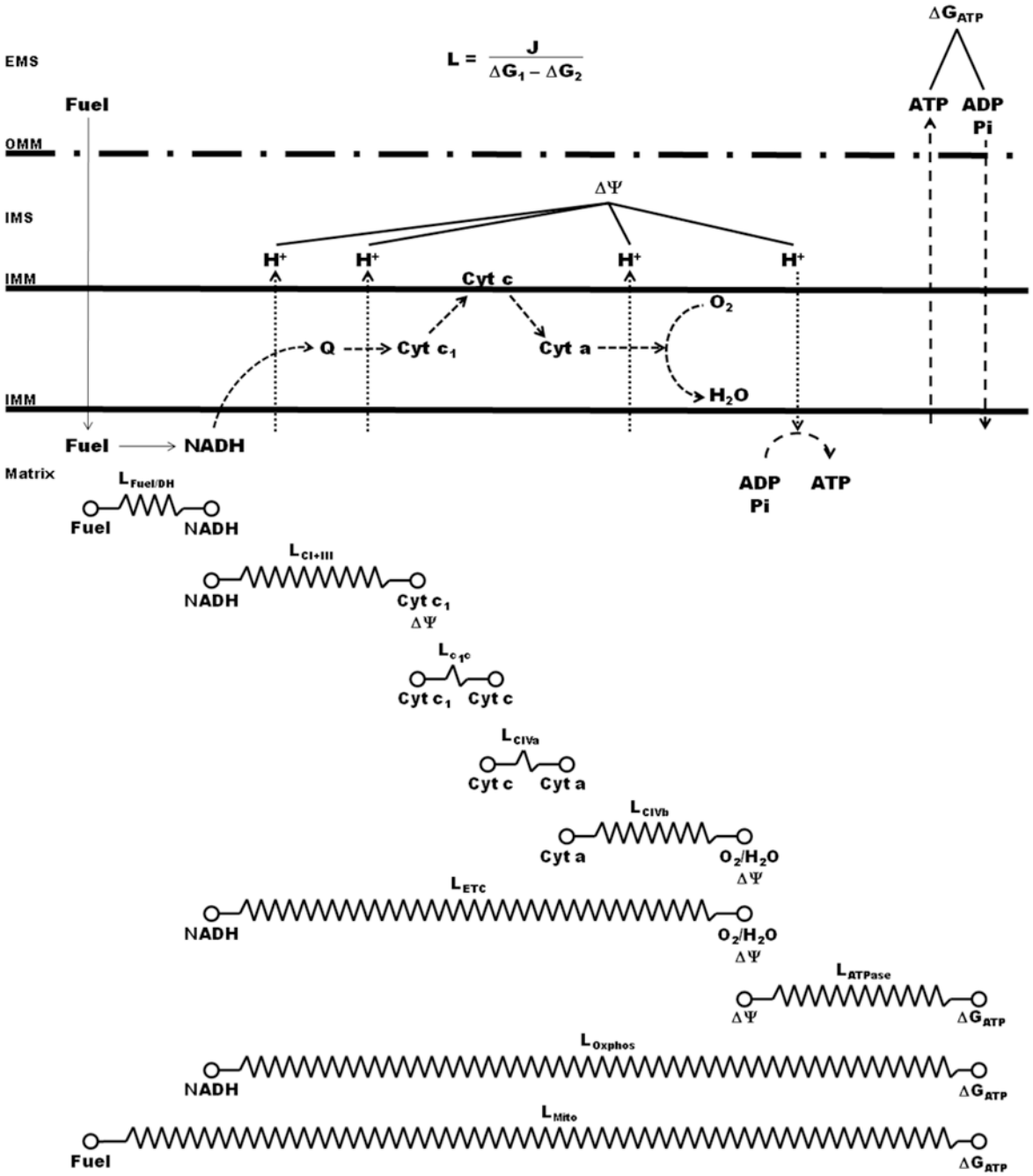

Figure 5.

Simple model of the mitochondrial energy conversion cascade. The path of energy flow is depicted in the top half of the figure while the measured energetic driving forces and how they relate to the calculation of conductances or resistances is depicted in the lower portion of the figure.

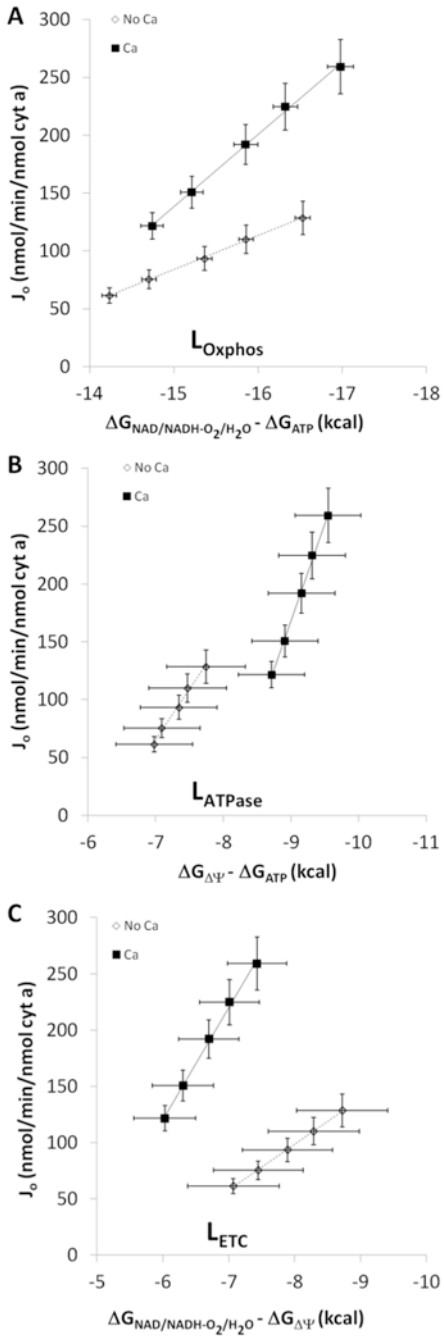

Figure 6.

Effect of calcium on mitochondrial conductances. A: Relationship between J_o and the free energy difference between NADH and ΔG_{ATP} with and without calcium. B: Relationship between J_o and the free energy difference between $\Delta\Psi$ and ΔG_{ATP} with and without calcium. C: Relationship between J_o and the free energy difference between NADH and $\Delta\Psi$ with and without calcium. Filled squares – calcium, open diamonds – no calcium. Error bars signify standard error. n = 12. Slopes, regression analyses, and the resultant p-values for A, B, and C are reported in Table 2 under L_{Oxphos}, L_{ATPase}, and L_{ETC}, respectively.

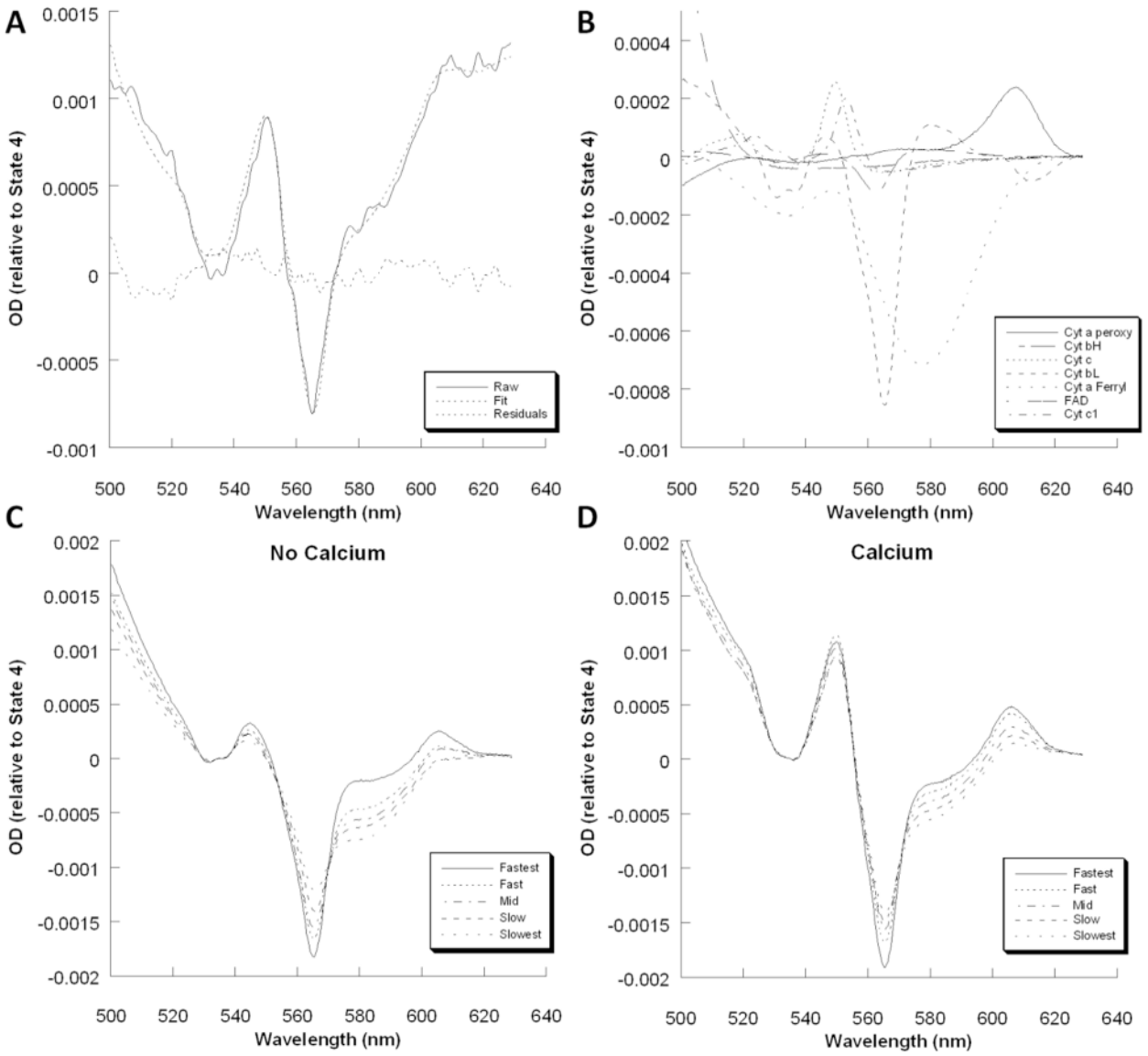

Figure 7.

Representative spectra and fits for mitochondrial cytochromes. A: Representative raw, fit, and error residual spectra of a transition from State 4 to intermediate respiration. B: Individual cytochrome components of the fit spectrum from A. C: Representative fit spectra from a CK clamp experiment without calcium. D: Representative fit spectra from a CK clamp experiment with calcium.

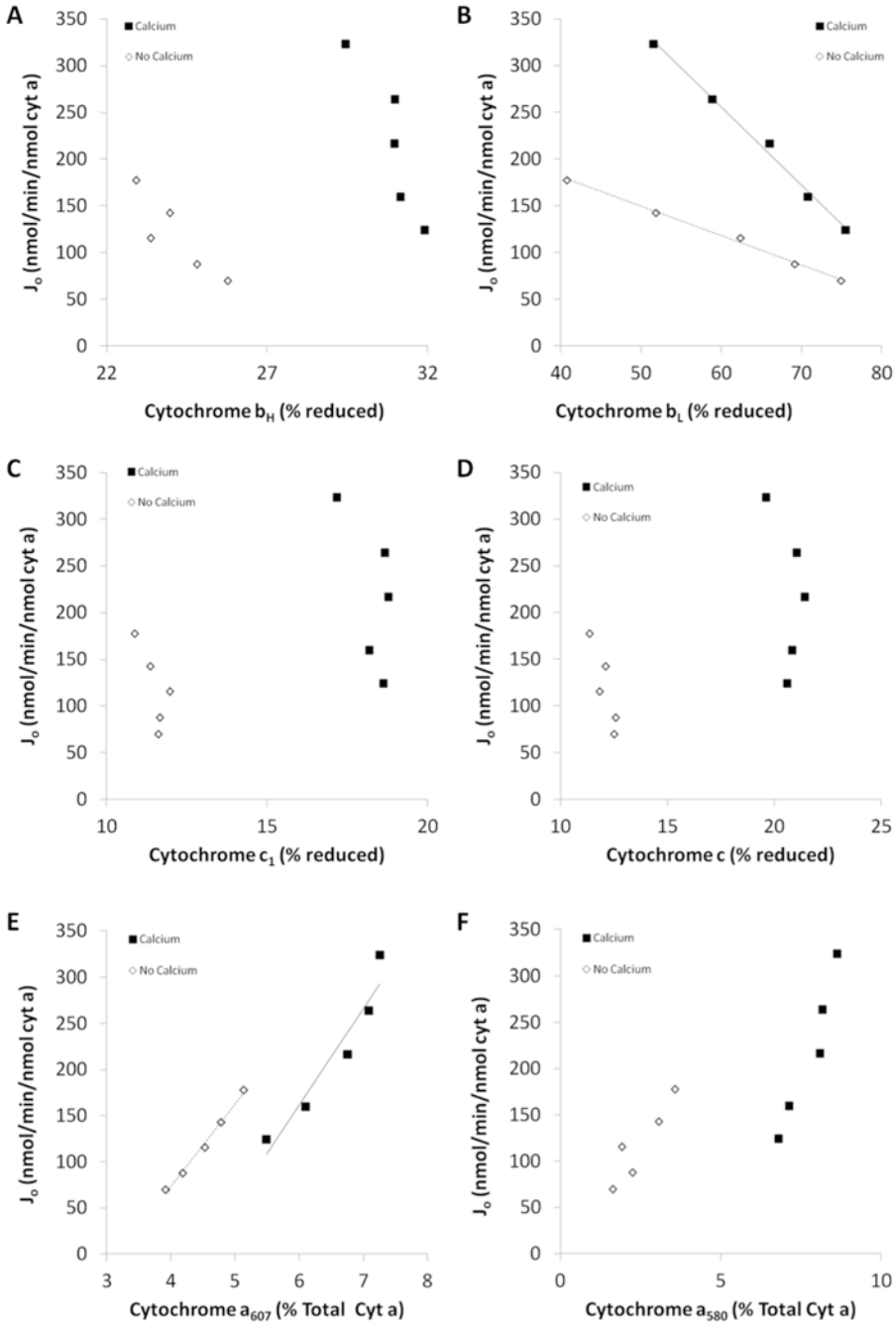

Figure 8.

Effect of calcium on the kinetic relationship between cytochrome redox state and flux. A: Relationship between cytochrome b_H and J_o with and without calcium. B: Relationship between cytochrome b_L and J_o with and without calcium. C: Relationship between cytochrome c_1 and J_o with and without calcium. D: Relationship between cytochrome c and J_o with and without calcium. E: Relationship between cytochrome a_{607} and J_o with and without calcium. F: Relationship between cytochrome a_{580} and J_o with and without calcium. Filled squares – calcium, open diamonds – no calcium. Trendlines are included for

relationships with R^2 values above 0.8. n = 4. Slopes, regression analyses, and the resultant p-values are reported in Table 2.

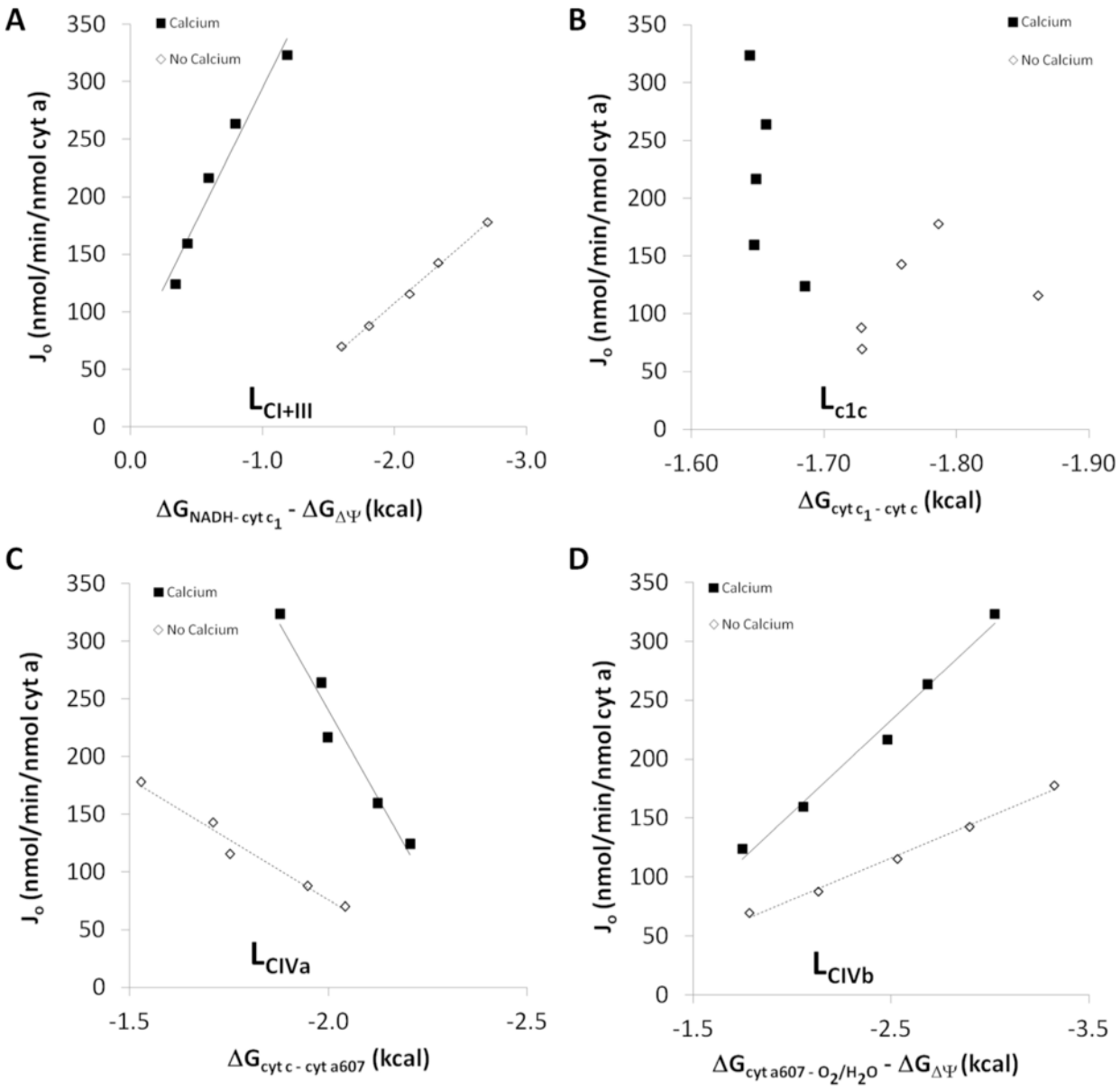

Figure 9.

Conductances within the electron transport chain. A: Conductance of electron flux between NADH and cytochrome c_1 with and without calcium. B: Conductance of electron flux between cytochromes c_1 and c with and without calcium. C: Conductance of electron flux between cytochromes c and a_{607} with and without calcium. D: Conductance of electron flux between cytochrome a_{607} and O_2 with and without calcium. Filled squares – calcium, open diamonds – no calcium. Trendlines are included for relationships with R^2 values above 0.8. n = 4. Slopes, regression analyses, and the resultant p-values are reported in Table 2 for A-D as L_{CI+III}, L_{c1c}, L_{CIVa}, and L_{CIVb}, respectively.

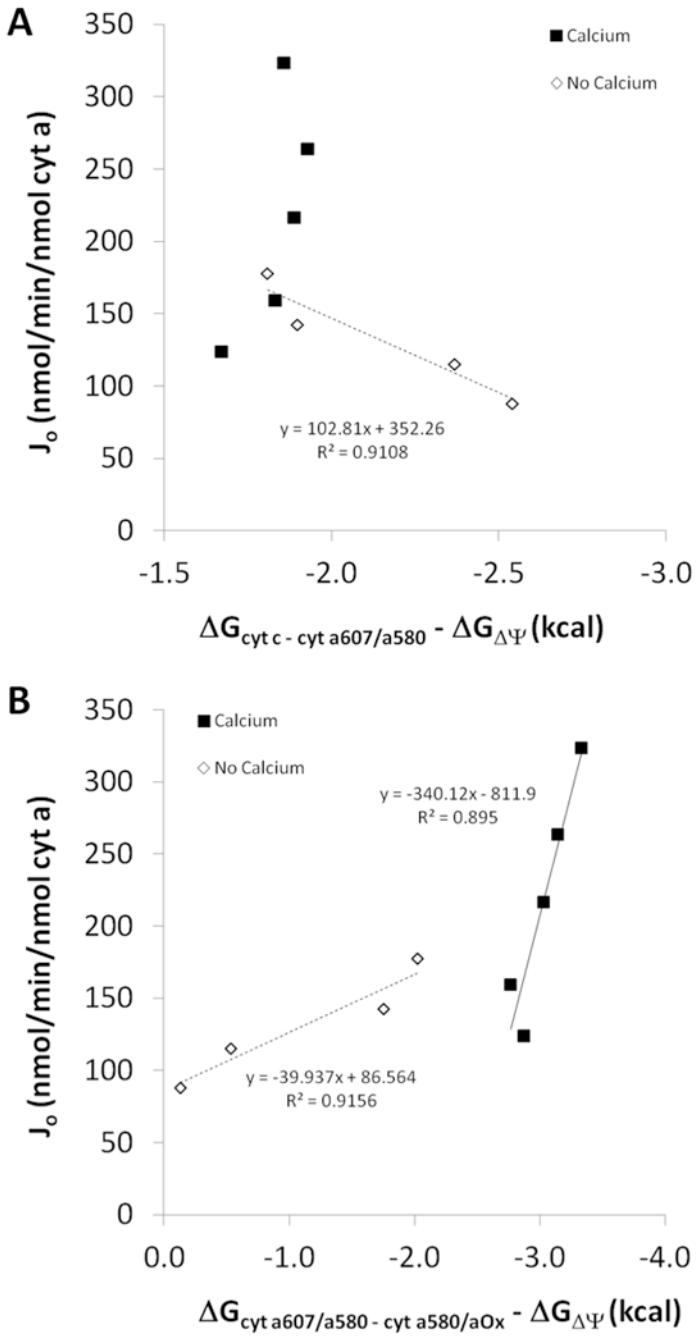

Figure 10.

Conductance of electron transfer within Complex IV. A: Conductance of electron flux between the cytochrome c and cytochrome a_{607}/a_{580} redox couples. B: Conductance of electron flux between the cytochrome a_{607}/a_{580} and cytochrome a_{580}/oxidized redox couples. Filled squares – calcium, open diamonds – no calcium. Trendlines are included for relationships with R^2 values above 0.8. n = 4.

Table 1

Oxygen Consumption, NADH % Reduction, and Membrane Potential at Maximal and Resting Respiration

Incubation Conditions	J_o		NADH		ΔΨ	
	State 4	State 3	State 4	State 3	State 4	State 3
No Calcium (n=9)	31.0 ± 3.2	226.8 ± 17.5^{+}	59.9 ± 5.1	17.8 ± 1.3	-202.1 ± 2.6	-171.5 ± 4.1
Calcium (n=9)	39.8 ± 3.1*	405.9 ± 12.6^{*+}	72.4 ± 2.9*	30.0 ± 1.3*	-203.1 ± 1.5	-174.9 ± 2.2
No NaCl, No Depletion, No Calcium (n=12)	29.3 ± 3.7	463.2 ± 19.0				

Skeletal muscle mitochondria oxidizing 10 mM glutamate and 1 mM malate. Values are means ± SE.

*denotes significant difference between Calcium and No Calcium.

$^{+}$denotes significant difference from No Depletion condition. J_O values are in nmol O_2/min/nmol cyt a. NADH values are % reduced. ΔΨ values are in mV.

Table 2

Mean Values for Force:Flow Relationships in Figures 3, 4, 6, 8, and 9

	Slope		r^2		
	No Calcium	**Calcium**	**No Calcium**	**Calcium**	**p-value**
NADH (mV)	12.2 ±2.6	20.5 ±4.0*	0.981 ±0.004	0.960 ±0.013	0.010
Cyt b_H (% reduced)	16.0 ±2.9	-75.6 ±40.5	0.518 ±0.192	0.558 ±0.200	0.108
Cyt b_L (% reduced)	-3.0 ±0.2	-8.2 ±1.1*	0.961 ± 0.006	0.937 ±0.018	0.021
Cyt c_1 (% reduced)	-15.9 ±27.7	-31.8±21.2	0.527 ±0.168	0.268 ±0.139	0.587
Cyt c (% reduced)	-53.6 ±10.5	-16.1 ±53.0	0.568 ±0.119	0.498 ±0.109	0.518
Cyt a_{607} (% total cyt a)	67.9 ± 17.9	87.8 ±32.5	0.937 ±0.022	0.893 ±0.053	0.678
Cyt a_{580} (% total cyt a)	4.6± 13.1	95.2 ±24.4	0.528 ±0.235	0.799 ±0.055	0.073
$\Delta\Psi$ (mV)	10.3± 1.4	22.1 ±2.5*	0.989 ±0.004	0.989 ±0.002	0.000
ΔG_{ATPe} (kcal/mol)	80.0 ± 11.3	163.2 ±17.9*	0.991 ±0.002	0.990 ±0.002	0.000
K_{mADp}(μM)	42.3 ±6.6	44.4 ±6.3	0.963 ±0.010	0.942 ± 0.023	0.687
$L_{Fuel/DH}$	-263.5 ± 57.3	-445.3 ±87.1*	0.981 ±0.004	0.960 ±0.013	0.010
L_{cl+iii}	-101.9 ±20.9	-224.7 ± 17.0*	0.992 ±0.001	0.927 ±0.043	0.012
L_{c1c}	-91.0 ±116.2	269.3 ±191.7	0.228 ± 0.078	0.122 ±0.081	0.266
L_{CIVa}	226.4 ± 56.0	543.7 ±46.3*	0.935 ±0.016	0.856 ± 0.064	0.043
L_{CIVb}	-55.8 ±13.5	-123.8 ±25.9*	0.989 ±0.004	0.970 ±0.021	0.036
L_{ETC}	-39.3 ±5.6	-96.0 ±11.1*	0.988 ±0.005	0.980 ±0.008	0.000
L_{ATPase}	-79.5 ±37.1	-192.5 ±33.7*	0.889 ±0.035	0.969 ±0.010	0.005
L_{Oxphos}	-29.8 ±4.8	-60.9 ±7.9*	0.989 ±0.003	0.990 ±0.003	0.000
L_{Mito}	-29.6 ±4.2	-60.4 ± 6.6*	0.991 ± 0.002	0.990 ±0.002	0.000

Values are means ± SE.

* denotes significantly different from No Calcium condition.

P-value compares No Calcium and Calcium slopes.

Table 3

Contribution of Each Pathway to the Total Mitochondrial Resistance to Energy Transfer

	Fuel Transport/Dehydrogenases	Complex I+III	Complex IV	ATP Production/Transport	Total Resistance (Ohms/nmol cyt a)
No Calcium	10.4 ± 0.8% (467)	27.1 ± 2.4% (1211)	37.7 ± 3.3% (1685)	24.7 ± 4.0% (1106)	4471 ± 558
Calcium	14.8 ± 3.2% (345)	21.2 ± 2.5%* (495)	30.5 ± 3.6%* (711)	29.1 ± 4.1%* (678)	2332 ± 441*

The mitochondrial energy conversion process was considered as a series of resistors where the total resistance is the sum of the individual parts. Resistance was calculated as the reciprocal of conductance and assuming 1 nmol O_2 = 4 × 6.02e^{14} electrons, 6.24e^{18} electrons = 1 coulomb and 23.062 V = 1 kcal/mol. N = 8.

* denotes significantly different from No Calcium. Values are means ± SE with mean resistance in Ohms/nmol cyt a in parentheses.

Table 4

Thermodynamic Stoichiometries for Individual Spans of the Electron Transport Chain

Stoichiometry	Ox Phos Span	Measured		Used	% Difference	
		No Ca	Ca		No Ca	Ca
H^+/e^-	NADH to cyt c_1	3.9 ± 0.0	3.8 ± 0.0	4.0	-2.5	-5.0
	Cyt c_1 to cyt c	0.1 ±0.0	0.1 ±0.1	0.0	-	-
	Cyt c to cyt a_{607}	0.3 ±0.0	0.3 ±0.0	0.0	-	-
	Cyt a_{607} to O_2	1.1 ±0.1	1.1 ±0.0	1.0	10.0	10.0
	NADH to O_2[#]	5.4 ±0.1	5.2 ±0.1	5.0	8.0	4.0
	NADH to O_2[*]	5.4 ±0.1	5.3 ±0.0	5.0	8.0	6.0

[#]Measured values are the sum of NADH to cyt c_1, cyt c_1 to cyt c, cyt c to cyt a_{607}, and cyt a_{607} to O_2.

[*]Measured values are from NADH to O_2 directly. N = 4.